NBS TECHNICAL NOTE 531

ARPA-NBS Program of Research on High Temperature Materials and Laser Materials

Reporting Period
July 1 to December 31, 1969

U.S.
RTMENT
OF
MMERCE
National
Bureau
of
Standards

NATIONAL BUREAU OF STANDARDS

The National Bureau of Standards was established by an act of Congress March 3, 1901. Today, in addition to serving as the Nation's central measurement laboratory, the Bureau is a principal focal point in the Federal Government for assuring maximum application of the physical and engineering sciences to the advancement of technology in industry and commerce. To this end the Bureau conducts research and provides central national services in four broad program areas. These are: (1) basic measurements and standards, (2) materials measurements and standards, (3) technological measurements and standards, and (4) transfer of technology.

The Bureau comprises the Institute for Basic Standards, the Institute for Materials Research, the Institute for Applied Technology, the Center for Radiation Research, the Center for Computer Sciences and Technology, and the Office for Information Programs.

THE INSTITUTE FOR BASIC STANDARDS provides the central basis within the United States of a complete and consistent system of physical measurement; coordinates that system with measurement systems of other nations; and furnishes essential services leading to accurate and uniform physical measurements throughout the Nation's scientific community, industry, and commerce. The Institute consists of an Office of Measurement Services and the following technical divisions:

Applied Mathematics—Electricity—Metrology—Mechanics—Heat—Atomic and Molecular Physics—Radio Physics [2]—Radio Engineering [2]—Time and Frequency [2]—Astrophysics [2]—Cryogenics.[2]

THE INSTITUTE FOR MATERIALS RESEARCH conducts materials research leading to improved methods of measurement standards, and data on the properties of well-characterized materials needed by industry, commerce, educational institutions, and Government; develops, produces, and distributes standard reference materials; relates the physical and chemical properties of materials to their behavior and their interaction with their environments; and provides advisory and research services to other Government agencies. The Institute consists of an Office of Standard Reference Materials and the following divisions:

Analytical Chemistry—Polymers—Metallurgy—Inorganic Materials—Physical Chemistry.

THE INSTITUTE FOR APPLIED TECHNOLOGY provides technical services to promote the use of available technology and to facilitate technological innovation in industry and Government; cooperates with public and private organizations in the development of technological standards, and test methodologies; and provides advisory and research services for Federal, state, and local government agencies. The Institute consists of the following technical divisions and offices:

Engineering Standards—Weights and Measures — Invention and Innovation — Vehicle Systems Research—Product Evaluation—Building Research—Instrument Shops—Measurement Engineering—Electronic Technology—Technical Analysis.

THE CENTER FOR RADIATION RESEARCH engages in research, measurement, and application of radiation to the solution of Bureau mission problems and the problems of other agencies and institutions. The Center consists of the following divisions:

Reactor Radiation—Linac Radiation—Nuclear Radiation—Applied Radiation.

THE CENTER FOR COMPUTER SCIENCES AND TECHNOLOGY conducts research and provides technical services designed to aid Government agencies in the selection, acquisition, and effective use of automatic data processing equipment; and serves as the principal focus for the development of Federal standards for automatic data processing equipment, techniques, and computer languages. The Center consists of the following offices and divisions:

Information Processing Standards—Computer Information — Computer Services — Systems Development—Information Processing Technology.

THE OFFICE FOR INFORMATION PROGRAMS promotes optimum dissemination and accessibility of scientific information generated within NBS and other agencies of the Federal Government; promotes the development of the National Standard Reference Data System and a system of information analysis centers dealing with the broader aspects of the National Measurement System, and provides appropriate services to ensure that the NBS staff has optimum accessibility to the scientific information of the world. The Office consists of the following organizational units:

Office of Standard Reference Data—Clearinghouse for Federal Scientific and Technical Information [3]—Office of Technical Information and Publications—Library—Office of Public Information—Office of International Relations.

---

[1] Headquarters and Laboratories at Gaithersburg, Maryland, unless otherwise noted; mailing address Washington, D.C. 20234.
[2] Located at Boulder, Colorado 80302.
[3] Located at 5285 Port Royal Road, Springfield, Virginia 22151.

UNITED STATES DEPARTMENT OF COMMERCE
Maurice H. Stans, Secretary
NATIONAL BUREAU OF STANDARDS • Lewis M. Branscomb, Director

NBS TECHNICAL NOTE 531

ISSUED JUNE 1970

Nat. Bur. Stand. (U.S.), Tech. Note 531, 75 pages (June 1970)
CODEN: NBTNA

ARPA-NBS Program of Research on High Temperature Materials and Laser Materials

Reporting Period
July 1 to December 31, 1969

Edited by A. D. Franklin and H. S. Bennett

Inorganic Materials Division
Institute for Materials Research
National Bureau of Standards
Washington, D.C. 20234

Supported by the
Advanced Research Projects Agency
of the Department of Defense

For sale by the Superintendent of Documents, U.S. Government Printing Office, Washington, D.C., 20402.
(Order by SD Catalog No. C13.46:531). Price 70 cents.

TABLE OF CONTENTS

Table of Contents (continued)

ARPA-NBS PROGRAM OF RESEARCH ON

HIGH TEMPERATURE MATERIALS AND LASER MATERIALS

Work Performed at the National Bureau of Standards

Supported by the Advanced Research Projects Agency,

Department of Defense

Reporting Period 1 July to 31 Dec., 1969

High Temperature Materials Reports Edited by A. D. Franklin
Laser Materials Reports Edited by Herbert S. Bennett

Brief reviews are given of work performed during the period July 1 to December 31, 1969, on a number of projects concerned with High Temperature Materials and with Laser Materials. Under the High Temperature Materials heading, topics include diffusion of oxygen in oxides, growth of Al_2O_3 crystals by chemical vapor deposition, the electronic structure of transition metal borides and related compounds, the optical constants of titanium, high temperature creep in copper, and the mechanism of volatilization of polymers and long-chain compounds. Work on Laser Materials includes measurement of bulk optical and elastic properties of laser materials, a study of the "orange" degradation of ruby, measurements of sub-crystal misalignment in ruby, damage in glass induced by high-energy laser pulses, chemical analyses for ruby and Nd-doped laser glasses, and preliminary studies on detection of submicroscopic inhomogeneities in glass.

Key words: Band structure, chemical analysis, copper, creep, crystal defects, crystal growth, diffusion, evaporation, glass, high temperature materials, inhomogeneities in glass, laser damage, laser glass, lasers, mass transport, materials properties, metal properties, optical properties, opto-elastic properties, oxides, polymers, ruby, titanium and transition.

1. INTRODUCTION

The National Bureau of Standards, with the support of the Advanced Research Projects Agency (Office of Materials Sciences) of the Department of Defense, is carrying out a program of research on High Temperature and Laser Materials. This program includes projects on the preparation and characterization of research-worthy materials; on the development of measurement techniques for and on the acquisition of critically needed data; and on the basic mechanisms controlling properties contributing to or limiting the use of materials at high temperatures. A summary of the results achieved in the period July 1 to December 31, 1969, is given here.

2. OBJECTIVES

The development of Defense technology often is limited by the properties of the available materials. When such a limitation is met, it generates a search for ways to improve the properties of existing materials or to find new and better ones. Such a search is like a military campaign - objectives must be set and a strategy devised to reach the objectives. Thus the devising of the strategy guiding the search for a new or improved material is a key part of DoD operations. If DoD is to continue to meet its commitments, it cannot neglect the development now of adequate strategies to meet future but foreseeable problems.

In order to devise a successful strategy, a great deal of background information about the behavior of materials in a given class may be needed, even though at times this information is used in subtle ways. A case in point is the development of missile-grade graphite* by DoD, 1957-1963.

As a result of previous basic studies of graphite, a good deal was known about the fundamental properties of this material, and this information acted as guidelines in a concentrated, deliberate and successful attempt by DoD to

---

*See MAB-222-M, Report of the Ad-hoc Committee on Principles of Research-Engineering Interaction, July 1966 for details of this development.

find industrial processes whereby graphite could be produced with optimum properties and high reproducibility for missile use.

In this sense of providing support for the strategy for the development of needed materials, the present program has come to focus upon two problem areas, Diffusion in Oxides, and Properties of Laser Materials. The ARPA support for the other areas listed in the Table of Contents in this Report is being phased out, and will for the most part cease with the present reporting period, although the work on Properties of Refractory Borides, which is included in a separate proposal to ARPA, may be continued for another six months.

3. HIGH TEMPERATURE MATERIALS PROGRAM

3.1. Objectives in High Temperature Materials

The operation of rocket and jet engines involves exposing metals at high temperatures to oxidizing conditions, and raises the problem of oxidation protection of high temperature refractory metal structural components. This same problem, currently for superalloy turbine blades, is posed again by jet engines. The oxidation protection of metals requires some form of barrier layer to prevent diffusion. This layer, either applied or developed by the early stages of oxidation itself, will most likely be an oxide, and will function to keep the metal and oxygen apart. It can work only if the diffusion rates of oxygen and metal atoms through the layer are small enough. Thus the strategy for the development of oxidation protection of otherwise susceptible metals at high temperatures will depend in part on being able to control the rates of diffusion, and therefore, in having data on the diffusion rates themselves.

Diffusion in oxides is important to other classes of DoD problems. Thus improvements in the reliability and efficiency of military communication, computer, and radar circuitry could be made if ceramic magnetic and ferroelectric components could be made more reproducible and reliable. Because such important properties as initial susceptibility and coercive force of ferrites, and dielectric and peizoelectric properties of ceramic ferroelectrics are very sensitive to the microstructural features (porosity, grain size) controlled by sintering, the strategy for improvement here requires control over sintering in these ceramics. The same is true of the ballistic response of ceramic armor. The development of transparent armor requires new techniques for the suppression of grain growth during otherwise complete sintering, mainly of Al_2O_3.

Since sintering in ceramics is mainly brought about by diffusion processes, the development of successful, long-range strategies needed to meet these DoD needs rests in part on knowledge of the rates of diffusion of metal and oxygen atoms in oxides.

Reliable techniques for measuring oxygen diffusion rates are not yet available, and therefore reliable data for oxygen diffusion does not exist for any save a few oxides. Thus one objective of this program is to develop a reliable technique for measuring the rate of diffusion of oxygen in oxides.

Further, diffusion rates are notoriously sensitive to impurities, and strategies for control require knowledge of the basic rate in the pure material and of the way various classes of impurities influence it. This in turn requires very pure crystals for study. To date, almost no oxide crystals have been prepared pure enough to reveal the intrinsic diffusion rates. The second objective in this area is to prepare intrinsically pure crystals of Al_2O_3, one of the leading ceramic armor candidates.

3.2. Project Summaries in High Temperature Materials

3.2.1. Diffusion in Oxides

3.2.1.1. Measurement of Diffusion Coefficients in Oxides

A. L. Dragoo
Inorganic Materials Division
Institute for Materials Research

The objectives of this program are to develop a reliable technique for the measurement of the rates of diffusion of oxygen in single crystal oxides, and to measure and interpret data on specific oxides. Experimentally these two objectives consist of (1) extending the sensitivity of present techniques so that the ^{18}O distribution ("concentration profile") in a single crystal sample can be measured, (2) comparing the results of these concentration profile measurements with the measurements of the rate of exchange of ^{18}O between the gas phase and the oxide crystal, (3) determining the dependence of the diffusion rate on temperature, oxygen partial pressure, and impurities in the solid, etc., and (4) obtaining reliable diffusion and exchange coefficients. The experimental results will provide the basis for determining the mechanisms for oxide ion diffusion in the oxide studied. Currently, rutile (TiO_2) is the oxide of interest. A mass spectrometer is being used to determine isotope ratios.

Almost all work on the project during the past months has been focused on the construction of the inlet system for the isotope ratio mass spectrometer — consisting of roughing and high vacuum manifolds, sample and reference transfer lines, sample and reference storage, manometers and molecular leak inlet. The system has the capacity for three oxygen references and four carbon dioxide references of different isotopic composition. Oxygen samples on the order of 0.3 standard cc can be transferred from the diffusion furnace, stored and analyzed. It will be possible to convert the oxygen to CO_2 using a graphite filament before analysis with the mass spectrometer or to analyze it directly.

3.2.1.2. Crystal Growth from Vapor

H. S. Parker and C. A. Harding

Inorganic Materials Division
Institute for Materials Research

The objectives of this program are, first, the growth of aluminum oxide mono- and bicrystals of sufficient physical perfection and chemical purity for use as research materials; second, the reduction of both cation and anion impurities in vapor grown aluminum oxide crystals to sufficiently low levels to permit meaningful property measurements at the intrinsic level; and third, the extension of the technique to other materials of interest.

During this reporting period, work has continued on the growth of bicrystals containing symmetrical tilt boundaries, primarily devoted to an investigation of possible variations in the growth technique designed to reduce or eliminate the occasional veils which form in the crystal when the growth cycle is interrupted. The use of a brief etching period of 30 to 45 minutes duration at the beginning of each growth cycle, during which only hydrogen and chlorine are passed over the crystal, appears to be sufficient. However, attempts to utilize this etching on the original seed crystals have shown that chemical polishing in phosphoric acid is still required to completely remove mechanical damage resulting from sawing and grinding the seed plates.

Additional bicrystal specimens have been supplied to Dr. Heuer at Case Western Reserve University for use in the ARPA program on Mass Transport in Oxides.

Much of the effort has been devoted to the problem of improving the chemical purity of the crystals by changes in the technique and apparatus. Neutron activation analysis of representative samples has been completed and are compared

with the previously reported spectrochemical analysis in Table 1. Only four impurity elements were actually detected

Table 1
Chemical Analysis of NBS Vapor Grown Al_2O_3

Element	Spectrochemical Analysis	Neutron Activation Analysis
Cu	<10 ppm	0.027 - 0.038 ppm
Fe	questionable	<4 ppm[a/]
Ir	not detected	0.0005 - 0.002 ppm
Mg	<10 ppm	[b/]
Mn	<10 ppm	~0.0005 ppm
Sc	not detected	~0.015 ppm
Si	<10 ppm	[c/]
Cl	[c/]	0.1 ppm[a/]

a/ Detection limit, not observed in specimens
b/ Interference between ^{27}Al and ^{27}Mg, can not detect
c/ Could not be detected if present

by activation analysis: copper, iridium, manganese and scandium. The question of magnesium and silicon content remains unresolved and an alternative analytical technique will be required to determine the actual level of these impurities.

In Table 2, analyses of the aluminum metal used as a source material are given, both before and after use in the chlorinator. Comparison of these analyses with those of the crystals in Table 1 shows that considerable improvement in purity is inherent in the growth process. The comparison also suggests that, at the purity level under consideration, the aluminum may well be the chief source of contamination in the crystals. The marked reduction of silicon in the aluminum after use and its subsequent detection in the crystals indicates that this may be the most troublesome impurity. Reaction between the chlorine and metallic parts of the system is also evident from the new impurities found in the aluminum after use. The disappearance of gallium from the aluminum after use indicates that it also is being transported. A particular search was made in the crystals for gallium but if present, it is there at less than the 0.003 ppm level, the detection limit for activation analysis.

Table 2
Spectrochemical Analysis of Aluminum Source Material

Element	Material	
	Al Metal, as received, nominal 5N purity	Same, after use in Chlorinator
Ag	-	<10 ppm
B	<10 ppm	<10 ppm
Ca	questionable	-
Cr	questionable	questionable
Cu	10 - 100 ppm	10 - 100 ppm
Fe	10 - 100 ppm	10 - 100 ppm
Ga	100 - 1000 ppm	-
Mg	10 - 100 ppm	10 - 100 ppm
Mn	-	-
Ni	-	10 - 100 ppm
Pb	-	100 - 1000 ppm
Si	10 - 100 ppm	<10 ppm

A new furnace and chlorinator have been designed and are currently under construction. In this apparatus, contact between chlorine gas, aluminum chloride and metal parts will be minimized in order to reduce exposure to this source of contamination.

Single crystals of high purity Al_2O_3 have been provided in a cooperative effort to the ARPA Laser Materials Program at NBS for use in spin resonance studies where a chromium-free specimen was essential.

Plans for the next reporting period include completion of the new growth apparatus and continued emphasis on improvement in purity levels. The use of 6N aluminum as the source material will be tried. The possibility of utilizing spark source mass spectrometry to determine the silicon and magnesium levels will be investigated, as well as the use of NMR to determine, at least qualitatively, the hydrogen ion content of the crystals.

3.2.2. Properties of Refractory Borides

3.2.2.1. Electronic Structure of Refractory Hard Metals

J. R. Cuthill, L. H. Bennett, G. C. Carter
and A. J. McAlister

Metallurgy Division
Institute for Materials Research

The objective of this project is to study changes in the density of states upon compound formation, especially in high temperature borides. The information should contribute to the understanding of the basic principles leading to the design of high temperature alloys with prescribed properties. The class of compounds being considered in this study are those binary and pseudo-binary compounds characterized by one of the constituents having an incomplete d or f shell and the other constituent having no d or f electrons. The transition metal borides, aluminides, and beryllides are examples.

Information is being obtained in the present study from soft x-ray spectroscopy, nuclear magnetic resonance, Mossbauer spectroscopy, magnetic susceptibility, and other probes of the electronic density of states.

The efforts again this report period will be summarized under the following three general headings for the purpose of emphasizing their parallel importance: (1) Preparation and Characterization of Transition Metal Borides, (2) Physical Property Measurements of Transition Metal Borides, and (3) Electronic Structure Calculations.

1. Preparation and Characterization of Transition Metal Borides

The wide range in most physical property values in the literature to date, particularly on the transition metal borides, has been repeatedly pointed out to be due to the poor quality, inadequately characterized specimens from which the data were obtained. Mono- and diborides of the first, second, and third transition series metals made by what is generally accepted to be the best hot pressing and sintering technique, were found to be too high in carbon (>100 ppm). A modification of the method is now being tried.

In addition to the simple borides we are experimenting with mixed substitution type borides such as $(Cr_{1-x} V_x) B_2$ where the V might be expected to substitute for the Cr in all proportions and thereby provide an opportunity to study the effect of intermediate electron/atom ratios without

changing the crystal structure. Rather than mutually diffusing the previously prepared pure Cr and V diborides, which would require a very high temperature, a CrV alloy was made and ground to - 325 mesh. The alloy powder was pressed together with pure boron powder and sintered at 1500°C for 1 hour. Diffusion had progressed about 1/4 of the way into the center of the alloy grains. Good diffusion results might be obtained by this method but the development of extraneous second phases is still possible.

NMR has again provided us with critical specimen characterization information. The x-ray diffraction pattern of one of our ScB_2 specimens revealed the proper pattern of lines for ScB_2, plus a few additional weak unidentified lines. When this specimen was put into the NMR spectrometer the characteristic Knight shift for scandium metal was observed in addition to the Knight shift corresponding to ScB_2, indicating that the ScB_2 specimen was contaminated with excess scandium metal. After reheating the sample the resonance corresponding to elemental scandium metal was reduced. (Compare fig. 1a, showing both resonances before reheating, with fig. 1b, showing only the Sc in ScB_2 resonance. Note that the quadrupole effect in the Sc in ScB_2 resonance remains after the reheating.)

2. Physical Property Measurements

Of the boride rod specimens that we have acquired thus far the CrB and CrB_2 specimens would appear from the metallography, x-ray diffraction and nuclear magnetic resonance, to yield meaningful soft x-ray spectra. Some data on the Cr_M spectrum and the 4th order B_K spectrum has been obtained from the particular specimens which, as of this writing, permit some general features to be compared. The B_K 4th order spectra from both the CrB and CrB_2 peak are at the same energy and are of the same general width although it is evident that there are differences in the detailed shape of the bands. Neither does there seem to be any significant difference in the Cr_M peak position between the two compounds. A definitive study of the $M_{2,3}$ soft x-ray spectrum of pure chromium has been completed.[2] Corrections have been made for background, and sub-band and satellite overlap. The estimate of the pure Cr_M emission band thus obtained was compared with recent photoemission data and good correlation has been found.

We have obtained NMR Knight shift and quadrupole data on ScB_2, which is one of the few diborides upon which no previous measurements of such properties have been reported in the literature. This work has been completed between room temperature and 4°K. Both the Knight shift and the quadrupole coupling constant are the same at both temperatures. This, together with linewidth measurements, shows no

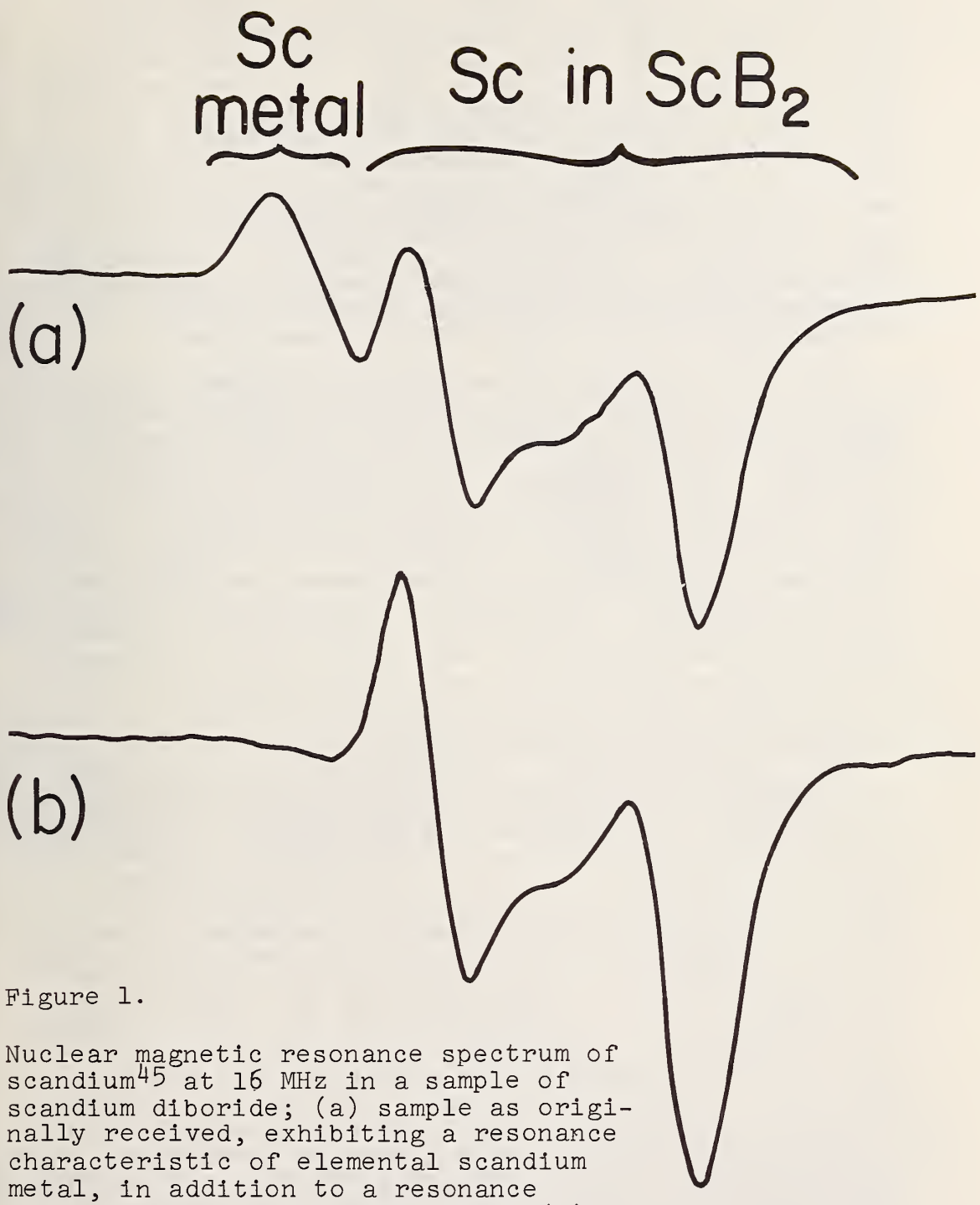

Figure 1.

Nuclear magnetic resonance spectrum of scandium^{45} at 16 MHz in a sample of scandium diboride; (a) sample as originally received, exhibiting a resonance characteristic of elemental scandium metal, in addition to a resonance corresponding to Sc in ScB_2, and (b) same sample after reheating and the elemental scandium metal resonance no longer discernible. The second order quadrupole effect present in the Sc in ScB_2 resonance is seen to remain after the reheating.

indications of magnetic behavior. The ^{11}B resonance is much as it is in the other diborides. The central line shows a little structure in the middle which does not disappear at higher frequencies (21 MHz). Our past experience tells us that much of this can be ascribed to noise arising from boron in the glass tube and, more importantly, the probe itself. With these limitations we find the Knight shift $K = 0.00\ (1)\%$* for ^{11}B, with respect to triethylborate. The quadrupole satellites are low in intensity, compared with, say CrB_2. This would suggest either a poor quality sample with large distributions of quadrupole interactions or the exciting possibility of an appreciable asymmetry parameter. The latter could have important consequences for understanding the crystallographic symmetries.

The ^{45}Sc resonances shows strong second order quadrupole effects. The value for e^2qQ/h, using second order quadrupole theory, coincides with that observed from the three pairs of satellites ($I^{45} = 7/2$), and has a value of 6.1(3) MHz. The linewidth of this resonance is proportional to $1/\nu$ so that the structure is due simply to second order quadrupole effects, without complications due to K_{ax}, which is also expected to be present for this hexagonal structure. The position for ν_0 was deduced from the position of the central ^{45}Sc resonance line, giving $K = +0.07(1)\%$ at both temperatures. This is in contrast to a negative Knight shift as observed for ^{51}V in VB_2, which has important implications regarding the electronic structure.

3. Electronic Structure Calculations

Generally the most solid progress is made when there is a parallel experimental and theoretical effort. Thus far the only work on borides has been experimental. There have been no electronic structure calculations on the mono- or diborides. Meanwhile, to explain experimental results there has been much discussion in the literature as to whether electrons are transferred from the metal to the boron or vice versa, or to the conduction band, etc., without anything being resolved. Therefore to complement the experimental program, computer routines are being prepared for augmented plane wave calculation of the band structure of the hexagonal diborides, XB_2, where X is a transition metal ion. It is these compounds which display metallic properties and high melting points, and are thus possibly of greatest technical interest. While these calculations are simple in principle, certain practical problems are encountered when studying compounds, and these are further complicated by the presence of transition metal ions, and the hexagonal lattice structure. The problem is one of convergence in the reciprocal lattice expansion. The larger the basis necessary, the lengthier and more expensive will

* In this expression, K=0.00(1)%, the number in parentheses is the uncertainty in the measurement, and belongs in the last decimal place given for the quoted value. This expression is therefore equivalent to $K=(0.00\pm.01)\%$.

the calculations be. At the present stage, our investigation should be regarded as a feasibility study.

3.2.2.2. Reactivity of Borides

J. J. Ritter and T. D. Coyle

Inorganic Materials Division
Institute for Materials Research

This project was initiated in September, 1969. The principal objectives are to investigate the chemical reactivity of refractory borides and related materials toward selected families of reagents. The reagents to be used include interhalogen compounds (ClF_3, BrF_5, etc.) and noble gas fluorides (XeF_2), which, as powerful oxidizers, fluorinating agents, and non-aqueous solvents may afford extensive and structurally selective reactions. Initial emphasis will be placed on development of degradation techniques useful in chemical and isotopic analysis. Volatile intermediates produced in the reactions and related molecular compounds will be investigated as possible precursors and vapor transport reagents for synthesis of the refractory materials.

The initial work on this project has involved the design of laboratory facilities required for safe and rigorously controlled handling of the reagents and for precise and quantitative investigations of the reactions. The design has been completed, and necessary procurements have been initiated. Construction of apparatus will begin shortly after 1 January 1970.

3.2.3. High Temperature Metals

3.2.3.1. Optical Constants of Titanium

A. J. Melmed

Metallurgy Division
Institute for Materials Research

The objective of this project is to determine the optical constants (complex index of refraction) of titanium by ellipsometry at room temperature in the visible region of the light spectrum. It is recognized that titanium, at room temperature, is optically anisotropic and chemically reactive with the normal atmospheric environment. Therefore measurements in different crystallographic directions, under appropriate clean surface conditions are necessary for a proper determination of optical constants. In addition it is recognized that considerably more polycrystalline

titanium than single-crystal titanium is used outside of the laboratory, so that optical constants of poly-crystalline specimens will also be determined.

The new experimental tube described in the last report has been completed and tested. All aspects of the tube are functioning properly. However, a problem of specimen contamination with carbon was encountered. Efforts to eliminate the problem were begun early in the present report period, but were temporarily suspended due to scheduling difficulties. This project is being terminated, but it is hoped to complete at least some of the measurements in the future.

3.2.3.2. High Temperature Creep in Metals

A. A. O. Rukwied, W. A. Willard and D. E. Harne

Metallurgy Division
Institute for Materials Research

The objectives of this investigation are to investigate the microscopic mechanisms that control high temperature creep, i.e., creep occurring at temperature $T>T_m/2$, where T_m is the melting point. More specifically it is planned to study: (a) the effect of temperature on the creep rate and compare this to the temperature dependence of dislocation velocity, (b) the effect of stress and compare this to measurement of dislocation density carried out by etch pit techniques, (c) study the effect of stacking fault energy through its variation in an alloy series and (d) study the effect of grain boundaries by comparison of studies in single crystals and polycrystals. For these studies copper and copper-alloys have been selected to begin with especially since etch pit techniques for these materials are already developed.

In order to get a faster and more accurate evaluation of the experimental creep data on high purity copper, digital computer data processing was employed. The second stage true strain rates were determined using first and second order least square fitting techniques. For the derivation of the activation energies the slopes of the Arrhenius plots of $\ln\dot{\varepsilon}_s$ vs. $1/T$ (where $\dot{\varepsilon}_s$ is the second stage creep rate and T the absolute temperature) also were determined using linear least square fits.

The resulting value of the apparent activation energy for second stage creep was $Q_c = 39.5 \pm 1$ kcal/mol

(165±4 kJ/mol) for stress levels of 1000 and 1500 psi (6.89×10^6 and 10.34×10^6 N/m^2, respectively), only slightly less than the previously reported value of 42±1.5 kcal/mol (176±6 kJ/mol). However it turned out that another test series measured at a stress of 2250 psi (15.51×10^6 N/m^2), the minimum creep rates of which resulted in an apparent activation energy of 42.4 kcal/mol (177 kJ/mol), has to be considered with great caution with regard to its value of the apparent activation energy for steady state creep. It could be shown from the residual curvature of the fitted parabolic curves as well as from Andrade-type plotting of the creep curves ($\dot{\varepsilon}^*$ vs. $t^{1/3}$), that in these tests at the onset of third stage (leading to fracture) steady state was not quite reached yet.

The apparent activation energy for steady state creep, Q_c, is usually assumed to be identical with the thermodynamically defined enthalpy of activation, ΔH, which is measured as the temperature sensitivity of the strain rate at constant stress and structure, i.e.

$$Q_c = \Delta H = -R(\partial \ln \dot{\varepsilon} / \partial\, 1/T)_{\sigma,\ \text{structure}} \qquad (1)$$

Within this definition, correct values of ΔH are derived from steady state creep rates only if the structure in second stage is a function of stress only and is independent of temperature.

One can hope to get additional information with regard to this point by employing the differential temperature test method (ΔT-method), where the creep rates are measured immediately before and after a small and rapid change in test temperature, which does not allow the structure to change significantly.

Three such ΔT-tests were carried out on high purity copper at stresses of 1000, 1500, and 2250 psi (6.89×10^6 10.34×10^6, and 15.51×10^6 N/m^2) and temperatures of 672°, 540°, and 485°C, respectively. The temperature was dropped by about 20°C in each case and was measured by a thermocouple attached to the specimen. The values obtained for ΔH were 71, 67.5, and 65 kcal/mol (297, 283, and 272 kJ/mol), respectively. This clearly is at variance with the steady state measurements in the high temperature regime up to 700°C, where 39.5 kcal/mol (165 kJ/mol) was found. It also cannot be reconciled with the measurements of Barrett and Sherby, who obtained from steady state creep rates values of ΔH of 61 kcal/mol (255 kJ/mol) at temperatures $T > 600$°C, and of 29.5 kcal/mol (121 kJ/mol) at $400°C < T < 600°C$ (both

values of ΔH are computed from their published steady state strain rate data).

Moreover, in order to get further insight into the influence on high temperature creep of the purity of the test material, the grown-in substructure, and the pre-test annealing treatment, a test series on OFHC copper (nominal 99.99% Cu) at a stress of 1500 psi (10.34×10^6 N/m^2) was started, and a few ΔT-tests on both types of materials are being carried out presently. At this time these results are still inconclusive.

If, however, we apply to our data obtained by the ΔT-method the analysis of activation parameters as given by Schoeck, then we obtain for the high purity copper a value of the Gibbs free energy, ΔG, of 40 kcal/mol (167 kJ/mol). In computing ΔG, we have assumed that the rate controlling process is diffusion, thus having an activation volume of the order of one atomic volume. In this case in the relation for ΔG as given by Schoeck the term involving the activation volume can be neglected and the entropy contribution is wholly described by the temperature variation of the elastic modulus,

$$\Delta G = \Delta H - T\Delta S = \frac{\Delta H}{1 - (T/\mu)(d\mu/dT)} \qquad (2)$$

The temperature variation of the elastic modulus, μ, has been measured by Barrett and Sherby and by Köster.

The observed discrepancy of the activation enthalpies, ΔH, as derived from the steady state tests (39.5 kcal/mol, 165 kJ/mol) and from ΔT-tests ($\approx$ 70 kcal/mol, 293 kJ/mol), clearly indicates the need to check on the theory and/or its assumptions.

According to the theory of thermally activated dislocation processes, the activation enthalpy for the rate controlling process is determined by measuring creep rates at different test temperatures under conditions of constant structure. The term constant structure means that during a small change in test temperature, or at different test temperatures in the case of steady state testing, the number of defect configurations at which under the action of a given stress thermal activation of a dislocation segment can occur does not change. The structure, thus comprising all defect configurations in the body which determine its creep behavior, gives rise to a long range internal stress in the body. This internal stress depends on temperature through

the temperature variation of the elastic modulus. Therefore, for steady state type creep testing over a wide range of temperature, it seems doubtful that the assumption of constant structure is realistic. Then the activation enthalpy as determined from the slope of an Arrhenius plot of $\ln \dot{\varepsilon}$ vs. 1/T would be incorrect, since it would be based on a set of different structures. On the other hand, a ΔT-test would more likely measure creep rates at constant structure, assuming that the structure adjusts reasonably slowly at the new test temperature.

The previously reported study attempting to better characterize the nature of the cellular solidification substructure in the high purity material (99.999% Cu) was continued. Ion probe microanalysis, carried out at CAMECA and at Bell and Howell, could confirm the segregation of carbon and silicon at the cellular structure. Moreover, the presence of these elements in form of clusters or particles of about <10 nm (100 Å) size could be detected. Due to its high chemical affinity to the other possible contaminants (i.e., C and O) the silicon should be present in form of silicon oxide or carbide. It is obvious that such particles cannot be removed from solid copper by mechanical and/or thermal treatment. This explains the stability of the grown-in substructure, which in some way will interact with moving dislocations.

No time could be spent on the single crystal program.

3.2.4. Polymers

3.2.4.1. The Volatilization and Decomposition of Materials

L. A. Wall, S. Straus, and G. Mattamal

Polymers Division
Institute for Materials Research

No actually new compounds were studied in the past six months. Previous work was repeated. The energy of vaporization for the C_{94} n-alkane was checked by carrying out the measurement of its rate of vaporization at four different temperatures covering a larger temperature range than previously.

A final manuscript covering the alkanes, entitled "Rates of Molecular Vaporization of Linear Alkanes" by L. A. Wall, J. Flynn, and S. Straus has been submitted

to the Journal of Physical Chemistry for publication.

Another paper entitled "Vaporization of Organic Plasticizers" by L. A. Wall, J. H. Flynn, and S. Straus has now been published in Polymer Engineering and Science, Volume 10, page 19, January, 1970.

Finally, we have been synthesizing and purifying compounds for study. These include:

Series (1)	Series (2)
Tributyrin	Di n-butyl sebacate
Tricaproin	Di n-hexyl sebacate
Trictanoin	Di n-octyl sebacate
Tridecanoin	Di n-decyl sebacate
Trilaurin	Di n-dodecyl sebacate
Trimyristin	Di n-tetradecyl sebacate
Tripalmitin	Di n-hexadecyl sebacate
Tristearin	Di n-octadecyl sebacate

We have also obtained three dimethylsiloxane oligomers from Dr. Walter Zisman for study. The study of the vaporization of these compounds should give some new insights into our comprehension of vaporization phenomena.

4. LASER MATERIALS PROGRAM

4.1. Introduction to Laser Materials

The National Bureau of Standards, with support from the Advanced Research Projects Agency of the Department of Defense, is carrying out a program of research on laser materials. This program includes studies to characterize laser materials, to define and evaluate damage measurements in laser materials, and to investigate the degradation of laser performance. A summary of the results achieved during the reporting period is given here.

4.2. Objectives of Laser Materials

One of the important factors which is limiting the advance of ultra high power laser technology is the failure or degradation of laser materials due to optically induced damage. In the past, the empirical approach to laser materials has been adequate. That is, the damage or degra-

dation to laser materials has been circumvented by equipment design or by a cut-and-try improvement in the laser materials. This problem of optically induced damage now poses a serious threat to the successful application of laser devices to an important class of needs of the Department of Defense. This fact has been recognized and the Advanced Research Projects Agency supports research to improve the performance of laser materials. The convening within the last nine months of three committees to examine the optical damage to laser materials illustrates the present concern and importance of solving this class of problems. These committees are the Subcommittee II of ASTM Committee F-1, the Institute for Defense Analysis study, and the National Materials Advisory Board Committee on the Fundamentals of Damage in Laser Glass.

The success of these efforts depends upon having the knowledge and proper skills available when they are needed. In the case of laser technology, they include the science and techniques of laser materials preparation and characterization and of the measurement and evaluation of those properties which are relevant to the damage and degradation of lasers. It is the overall objective of the present NBS program on laser materials to identify some of the more important problems concerning damage and degradation of lasers and to provide the necessary advances in those areas for which NBS possesses the competence to do so. These efforts will be directed mainly toward providing the techniques for the preparation and characterization of laser materials to be used in tests for the measurement and evaluation of material properties pertinent to the damage and degradation of lasers, for the tabulation of key damage data, and for the improvement in the knowledge and skills necessary to advance the performance of lasers.

In pursuit of this program, a continuing attempt is being made to analyze the technological problems associated with high performance lasers and the materials from which they are constructed, and to distill from this analysis major scientific problems whose solutions would advance laser technology. In addition, the problems chosen should fall within areas in which NBS has available competence. Also, the number of problems included in the program should be kept small enough so that each one can be approached in a reasonably comprehensive manner.

In accordance with these criteria, the present program contains three subdivisions – Characterization of Laser Materials, Damage to Laser Materials, and Degradation of Laser Materials. Damage and Degradation as used here are distinguished in that Damage is localized and occurs during

the course of a very few pulses whereas Degradation implies the much more gradual and general deterioration of performance over many pulses. There may of course be some overlap.

4.3. Overall Summary of Projects on Laser Materials

4.3.1. Characterization of Laser Materials

There is a continuing need for the characterization of laser materials. Suppliers frequently make changes in composition and usually do not provide adequate data on those physical and chemical properties which influence laser performance and the distortion of wave fronts propagating in laser materials. The index of refraction, thermal change in the refractive index, elastic constants, photoelastic constants, thermal expansion, density, and chemical composition have been measured for five commercial Nd-doped laser glasses. The possibility of eliminating electrostrictive effects by judiciously altering the glass composition has been examined. A lithium-silicate laser glass whose composition approximates that of some commercially available laser glasses was found to have a consolute temperature between 440°C and 480°C. Since the consolute temperature occurs near the transformation region, a large degree of phase separation may occur during annealing. Other compositions will be examined in the future. The relation between phase separation and the performance of a laser is not understood very well and could require quantitative studies if one can show that phase separated glasses have consistently lower or higher tolerances to damage or degradation. X-ray diffraction techniques have been employed to characterize ruby laser rods and a correlation between crystal perfection and its performance in a laser has been considered.

4.3.2. Damage to Laser Materials

Inclusion damage (bulk) has been a serious source of difficulty for the laser systems engineer concerned with ultra-high power pulses. Although surface damage and intrinsic damage (self-focusing or beam trapping) contribute additional problems, these are at present apparently not as great an obstacle to the advance of laser technology as the inclusion damage is. A laser glass damage test facility is being constructed at NBS to study the damage problem and to attempt to bring some unity to the great proliferation of

damage data. This test facility will center around a one gigawatt neodymium laser system. Preliminary experiments on the damage of silica and glass samples by exposure to a Q-switched ruby laser pulse of 3 joules studied the variation of damage threshold with water content. These experiments also indicate that knowing the samples' total history is essential for interpreting and understanding the results of damage studies. The detection of incipient absorbing centers before they initiate a damage site would be most helpful in the chemical analysis of the site and its immediate neighborhood. Some ideas to detect incipient damage centers have been screened in a search for useful analytic methods. These include dielectric relaxation, nuclear magnetic resonance, azimuthal light scattering, forward light scattering, and infra-red detection techniques. None appear sufficiently promising to pursue at this time for the detection of inclusions leading to damage. Methods which employ optical interference or stress-birefringence principles have also been suggested. A theoretical model of an absorbing center in a laser glass host has been formulated. This model enables one to compute the space and time dependence of the temperature near the center, the thermal stress, and the stress-birefringence as functions of the laser pulse width, energy content of the laser pulse, and radius of the absorbing center. Preliminary computations indicate that such optical methods are promising.

4.3.3. Degradation of Laser Materials

At present, the coloration of some ruby and YAG laser rods after continued use is not well understood. The reasons are in part a lack of sufficient data on the differences among coloration by laser pump light, x-ray irradiation, and γ-ray irradiation. The causes responsible for degradation in performance of solid state lasers after continued use have been studied by electron paramagnetic resonance and by optical means. Good laser quality ruby and "orange" degraded ruby samples were examined by both their absorption spectra and their electron paramagnetic resonance. Also, particular attention has been given to the valence states of the chromium ions, magnesium ions in doubly doped rubies, and of impurity ions. Similar studies are planned for YAG crystals.

4.4. Individual Project Summaries

4.4.1. Characterization of Laser Materials

4.4.1.1. Physical and Chemical Properties of Laser Materials

G. W. Cleek and R. M. Waxler

Inorganic Materials Division
Institute for Materials Research

The objective of this project is to determine the physical properties of laser glasses and crystals and to relate these properties to their chemical composition.

Accomplishments

Measurements on five commercially-made Nd-doped laser glasses have been completed. Data were obtained on such properties as refractive index, thermal change in refractive index, elastic constants, photoelastic constants, thermal expansion, density, and chemical composition. These data are needed to calculate the corrections for the distortion of the wavefront in light generated by the lasers. The distortion is produced by thermal effects when the rods are operated. The results have been presented earlier in NBS Technical Note 514.

The photoelastic constants of single crystal ruby doped with 0.05 wt % of Cr_2O_3 have been determined and the results have been prepared for publication.

Chemical Analyses*

(1) Ruby Boules - Neutron activation analysis was used for the determination of trace impurities in three different ruby boules. The three boules were doped with Cr_2O_3 at nominal levels of 0.03, 0.05 and 0.064 wt %, respectively. For the 0.03% and the 0.064% boules, two adjacent samples from the same boule were analyzed.

The crystals were cut to obtain samples of a uniform thickness and similar cross-sectional area. Each sample was sealed in polyethylene and irradiated for 60 minutes in pneumatic tube RT-4 of the National Bureau of Standards Reactor at a power level of 10MW ($\sim 1 \times 10^{13}$ n-cm^{-2} sec^{-1}). This facility was chosen because of its higher ratio of thermal to fast neutrons over the facility used for previous analyses. The remainder of the procedure was identical to that reported previously in NBS Technical Note 514.

---

*Neutron activation analyses by Barbara A. Thompson, Analytical Chemistry Division

Table 1

Results of Activation Analysis of Ruby Crystals, ppm

Element	Crystal Designation "0.03%" #1	"0.03%" #2	"0.05%"	"0.064%" #1	"0.064%" #2
Cr ($Wt\%Cr_2O_3$)	0.0222	0.0215	0.0443	0.0442	0.0463
Ba	42.6	0.24	9.4	15.2	1.26
Sr	1.55	<0.2	0.41	0.49	0.066
Cu	0.075	0.062	0.070	0.026	0.060
Mn	0.0013	0.002	0.0012	-	0.0018
Ga	3.05	2.98	0.004	0.014	0.016
W	0.032	0.052	0.034	0.015	0.030
Ir	0.239	0.245	0.0255	0.0500	0.0539
Na	<2	<2	<2	<2	<2
Au	<0.0002	<0.0002	<0.0002	<0.0002	<0.0002
La	<0.002	<0.002	<0.002	<0.002	<0.002
Co	<0.02	<0.02	<0.02	<0.02	<0.02

The results obtained are shown in Table 1. All results are in ppm of the element except the Cr results which are reported as percent Cr_2O_3. The improved ratio of thermal to fast neutrons in the new irradiation facility resulted in a reduction of almost an order of magnitude in the ^{24}Na production from the reaction $^{27}Al(n,\alpha)\ ^{24}Na$. The measurement of short-lived activities such as ^{64}Cu, ^{72}Ga, ^{56}Mn, and ^{87m}Sr was thus made much more reliable. An upper limit for Na in the crystals is reported which takes into account the Na produced from the Al_2O_3 matrix. Because of interferences, the values for W in the table should probably be regarded as upper limits rather than firm concentrations. For the crystals containing nominally 0.03% and 0.064% Cr_2O_3, two adjacent samples were cut from each boule and in each case the sample designated #1 was from the wider end of the crystal.

(2) Neodymium-doped Laser Glasses - Five commercially-made specimens of neodymium-doped laser glasses were analyzed by neutron activation methods, with particular care taken to determine trace impurities.

These glasses are very complex mixtures, containing in some cases as many as ten principal constituents. For activation analysis the constituents representing the most serious interferences to the measurement of other activities are sodium, antimony (1% or more in 4 of the glasses), and neodymium (3-5%). The neodymium is especially aggravating since on irradiation it yields three radionuclides: ^{151}Nd, with a 12 minute half-life; ^{149}Nd, with a 1.8 hour half-life; and ^{147}Nd with an 11 day half-life. ^{151}Nd and ^{149}Nd also decay to form radioisotopes of promethium with half-lives of 28 hours and 53 hours.

To try to obtain the maximum amount of information with a reasonable expenditure of effort three sets of irradiations were carried out. For each of the glasses a small sample (10-50 mg) was irradiated for 2 seconds and used to determine Na, K, and Sb. A larger sample (100-200 mg) of each glass was irradiated for 1 minute, and dissolved in $HF-HClO_4$. After fuming to eliminate HF, the residue was taken up in 9N HCl and most of the antimony was removed by extraction into isopropyl ether. Sodium was then removed by passing the aqueous phase through a column of hydrated antimony pentoxide. The effluent was examined for low-level constituents of intermediate half-life. Those observed included La, Pr, Eu, and Sm. Common impurities such as copper and gallium were not observed.

A third set of samples (100-200 mg) was irradiated for 15 minutes and set aside for two weeks to allow all shorter-

lived activities to decay away. After dissolution and extraction of antimony as before the aqueous phase was counted and Nd, Ce, and Ba were determined (Glass E did not require these chemical separations since it had very low concentrations of Na and Sb).

All the samples were irradiated in the NBS Reactor at a flux of about 6×10^{13} n/cm^{2}sec. The maximum irradiation time-sample size combination was fixed by the ^{24}Na, ^{122}Sb - ^{124}Sb, and ^{147}Nd activities produced. All the samples were specially cut 1-mm thick slices. With samples this thin, neutron self-shielding was not a problem even for Glass E with 14% Li_2O. For this latter glass irradiation time was not limited by Na or Sb because these were quite low, but by Nd and by heating of the sample during irradiation by absorption of alpha particles from the reaction: ^{6}Li (n,α) ^{3}H. All the samples were rinsed in acetone and in dilute HNO_3 after irradiation to remove surface contamination. In most cases concentrations were determined by comparison to standards irradiated under the same conditions.

Results: The results obtained are given in Table 2. The relative standard deviation is estimated to be about ±5% in most cases. For the lower reported values of Sm there is severe interference from Nd and these values are probably no better than ±20%. For the lower reported values for Eu and Ce the signal-to-background ratio was poor and these values also are probably no better than ±20%. All results are reported as the oxide rather than the element to facilitate comparison with results from other methods.

Glass Composition and the Possibility of Eliminating Electrostrictive Effects

Several mechanisms for the cause of damage in laser materials have been considered during this period. In some of these mechanisms the effect is greatly enhanced by the presence of electrostrictive self-focusings, which lead to the formation of filaments. Chiao, Townes and Stoicheff [1] have pointed out that electrostrictive pressure is given by

$$p = (E^2/4\pi)\, n\, (\rho\, dn/d\rho), \qquad (1)$$

where E is the electric field, ρ the density of the material and n the refractive index. In addition, Chiao, Garmire and Townes [2] have shown that the refractive index changes due to the change in density caused by electrostriction are

Table 2

Results of Activation Analysis of Neodymium-Doped Glasses (wt%

	Glass A	Glass B	Glass C	Glass D	Glass E
Na_2O, %	6.9	7.8	3.2	6.4	0.044
K_2O, %	9.2	14.	17.	17.	<0.04
Sb_2O_3, %	0.90	0.86	2.5	0.93	0.0015
Nd_2O_3, %	5.5	5.8	3.5	5.7	3.5
BaO, %	5.1	3.3	3.5	2.8	<0.3
CeO_2, %	<0.006	0.005	<0.006	<0.006	0.521
La_2O_3, ppm	<0.9	10.	18.	7.8	<0.8
Pr_2O_3, ppm	<3	<3	<3	8.4	<2
Eu_2O_3, ppm	30.	0.6	$\leq$0.1	1.1	<0.5
Sm_2O_3, ppm	0.37	0.2	0.2	2.2	<0.03

given by

$$\Delta n = (E^2/4\pi)\, Bn\, (\rho\, dn/d\rho)^2, \qquad (2)$$

where B is the compressibility. It is obvious from equations (1) and (2) that the electrostrictive pressure will be zero and the change in index will be zero if $(\rho\, dn/d\rho) = 0$. The possibility of finding a material which will meet this condition has been studied, and the results are presented in this section of the report.

Data on $(\rho\, dn/d\rho)$ for various cubic crystals are available from studies conducted at NBS [3] and other laboratories [4,5] and these data are presented in Table 3. It can be seen that there is a considerable range in values of $(\rho\, dn/d\rho)$ from +1.31 for $PbNO_3$ to - 2.84 for GaAs. For the group of alkali halides there is a decrease in magnitude of $(\rho\, dn/d\rho)$ with increasing strength of interatomic binding. There are several crystals which have negative values of $(\rho\, dn/d\rho)$. With these crystals the refractive index becomes less under hydrostatic pressure because the decrease in polarizability of the constituent ions outweighs the positive contribution to index due to the increased number of scattering centers per unit volume [3,4].

In Table 3, it can be seen that YAG (Yttrium Aluminum Garnet) has a slightly negative value and very nearly fulfills the condition that $(\rho\, dn/d\rho) = 0$. A boule of undoped YAG has been obtained from Union Carbide Corporation, and it is planned to study the effect of high energy laser pulses upon the material. If equations (1) and (2) are correct, electrostrictive effects should be largely eliminated.

Although YAG is a promising material, the rod of a high energy pulsed laser will almost certainly have to be a glass, because the broad fluorescent line of a glassy host lends itself to Q-switching. In Table 4 values of $(\rho\, dn/d\rho)$ are given for several glasses. The first group shows values for 5 neodymium doped laser glasses which have been studied recently at NBS. The values are clustered closely around 0.34, although the Owens-Illinois glass has a slightly lower value, 0.30. The second group of 10 glasses were selected as being representative of 154 Schott glasses reported in a very thorough study by Schaeffer and Nassenstein [6]. The highest value is .77 for SFS1 and the lowest value is .24 for SSK8. In the third group are shown the results of experimental studies on simple glass compositions conducted at NBS. As_2S_3 has very high value of 2.34, and

Table 3

Values of $(\rho dn/d\rho)$ for cubic crystals*

Crystal	$(\rho dn/d\rho)$
KI	.44
KBr	.35
NaCl	.28
LiF	.13
NaF	.11
CaF_2	.25
YIG	.31
$PbNO_3$	1.31
MgO	-.31
ZnS	-.22
$SrTiO_3$	-.22
GaP	-1.90
GaAs	-2.84
YAG	-.01

* In the instances where the original data were reported in terms of Pockel's elasto-optic constants, p_{ij}, $(\rho\ dn/d\rho)$ was calculated according to the equation,

$$(\rho\ dn/d\rho) = \frac{n^3}{6}\,[p_{11} + 2p_{12}].$$

the calcium aluminate, F75, has a value of .19 which is significantly lower than the rest. The low value of (ρ dn/dρ) for the calcium aluminate glass (which contained 41.5 weight% Al_2O_3) is consistent with the fact that with applied hydrostatic pressure, crystalline Al_2O_3 (sapphire) exhibits a decrease in refractive index for both the ordinary and extraordinary ray [2,7].

Considering the fact there is a consistent trend toward negative values of (ρ dn/dρ) with increasing strength of interatomic binding for the group of alkali halides shown in Table 3, it is reasonable to assume that a similar trend holds for the series of alkaline earth oxides. It can be seen in Table 3 that MgO has a negative value of (ρ dn/dρ) so that substituting MgO for CaO in the calcium aluminate composition of F75 might be expected to reduce the value of (ρ dn/dρ) to one closer to zero. Moreover, according to the physical theory of photoelasticity, certain ions such as Be^{++} and F^- if substituted could be expected to make an even stronger negative contribution to (ρ dn/dρ) [4]. The electronic polarizability and binding strengths of the constituent ions are the important factors, and it should be possible to formulate some glass composition where (ρ dn/dρ) would equal zero.

In conclusion, it should be noted that the basic material parameters which describe the interaction between optical radiation and acoustic waves are Pockels' elasto-optic constants [4,8,9]. One of the mechanisms that have been proposed as the cause for laser damage in solid, transparent dielectrics is the generation of coherent ultrasonic phonons by stimulated Brillouin processes [1,10]. Chiao, Townes and Stoicheff [1] have pointed out that either compressional or shear waves may be excited, but for compression the coupling between acoustic and optical waves is simplest and may be described as electrostriction. In this case, equation (1) still holds. Chiao, Townes and Stoicheff have shown that, when the radiation is contained in a resonant cavity, the threshold condition for buildup of the acoustic and scattered wave is

$$\frac{E_o^2}{8\pi} \geq \frac{B}{2(\rho dn/d\rho)^2 \, k_s L_s \, k_{-1} L_{-1}}, \qquad (3)$$

where L_s and L_{-1} are the decay lengths of the sound and light waves respectively, and k_s and k_{-1} are the respective

Table 4

Values of $(\rho dn/d\rho)$ for glasses *

	Glass Type		$(\rho dn/d\rho)$
Neodymium-doped Laser Glasses	Glass A		.34
	Glass D		.34
	Glass B		.34
	Glass C		.36
	Glass E		.30
Schott Glasses	Fluoro Crown	FK1	.37
	Boron Crown	BK5	.33
	Crown	K4	.37
	Barite Crown	BaK5	.39
	Crown Flint	KF2	.34
	Dense Crown	SSK8	.24
	Barite Flint	BaF8	.46
	Flint	F9	.41
	Short Flint	KzF2	.43
	Special Dense Flint	SFS1	.77
NBS Experimental Glasses	Extra Dense Flint	F920	.81
	Fused As_2S_3		2.34
	Fused SiO_2		.32
	Fused GeO_2		.44
	Fused B_2O_3		.39
	Borate	E1583	.40
	Phosphate	F1329	.33
	Calcium Aluminate	F75	.19

* In the instances where the original data were reported in terms of Neumann's strain-optical constants, p and q, $(\rho dn/d\rho)$ was calculated according to the equation,

$$(\rho dn/d\rho) = \frac{n^2}{3} [q+2p].$$

propagation vectors of the sound and light waves. These authors have shown also that for the travelling wave case the threshold condition is

$$\frac{E_o^2}{8\pi} \geq \frac{B}{2(\rho dn/d\rho)^2} (L_s^{-1} + L_{-1}^{-1})^2. \qquad (4)$$

From equations (3) and (4) it can be seen that in a material where $(\rho\ dn/d\rho)=0$, the possibility of damage by stimulated Brillouin scattering is eliminated.

Refractive Index of Ruby

Three ruby boules, doped at nominal levels of 0.03, 0.05 and 0.064% of Cr_2O_3, respectively, were furnished by a commercial supplier. The crystallographic directions in the boules were determined by x-ray methods and prisms of known orientation were prepared for the refractive index measurements. The results are shown in Table 5.

Specimens cut from the same boules were analyzed by neutron activation methods and the results are given in Table 1. As may be seen from the table the boules containing nominal levels of 0.05% and 0.064% Cr_2O_3 were found to contain essentially the same amounts of Cr_2O_3. The refractive index values in Table 5 do not disagree with the analyses. The variations in refractive index for all three boules are only one or two in the fourth decimal.

When these measurements were planned it was expected that data would be obtained to allow the calculation of the change in refractive index produced by a change in the Cr_2O_3 concentration. Since the observed changes are so small no meaningful calculation can be made.

A comparison of these data with data reported in the literature on sapphire [11] and on ruby [12] show variations of two or less in the fourth decimal so that specimens containing appreciably more Cr_2O_3 would be required to determine the effect of Cr_2O_3 concentration on refractive index.

References

[1] R. Y. Chiao, C. H. Townes and B. P. Stoicheff, Phys. Rev. Letters 12 592 (1964).

Table 5

Refractive indices of ruby with different concentrations of Cr_2O_3 at 19.5°C

Wavelength (μm)	.03% Cr_2O_3 n_o*	.03% Cr_2O_3 n_e*	.05% Cr_2O_3 n_o*	.05% Cr_2O_3 n_e*	.064% Cr_2O_3 n_o*	.064% Cr_2O_3 n_e*
0.4047	1.7859	1.7774	1.7860	1.7776	1.7859	1.7775
0.4358	1.7813	1.7729	1.7814	1.7730	1.7813	1.7730
0.4678	1.7775	1.7692	1.7776	1.7693	1.7775	1.7693
0.4800	1.7762	1.7680	1.7764	1.7681	1.7763	1.7681
0.5086	1.7736	1.7654	1.7738	1.7656	1.7737	1.7655
0.5461	1.7708	1.7627	1.7710	1.7628	1.7709	1.7627
0.5876	1.7683	1.7602	1.7684	1.7603	1.7684	1.7603
0.6438	1.7655	1.7575	1.7657	1.7576	1.7656	1.7576
0.6678	1.7645	1.7565	1.7647	1.7566	1.7646	1.7566
0.7065	1.7631	1.7551	1.7632	1.7552	1.7633	1.7552

* n_o signifies ordinary, and n_e extraordinary, ray.

Preliminary data obtained by I. H. Malitson and M. J. Dodge.

[2] R. Y. Chiao, E. Garmie, and C. H. Townes, Proc. of the International School of Physics, Enrico Fermi Course XXXI, Academic Press, New York (1964) p. 326, "Raman and Phonon Masers".

[3] R. M. Waxler and C. E. Weir, J. Res. NBS 69A 325 (1965).

[4] R. S. Krishnan, Progress in Crystal Physics, Vol. 1, Interscience Publishers, New York, London (1959).

[5] K. Vedam and E. D. D. Schmidt, Phys. Rev. 146 548 (1966).

[6] C. Schaefer and H. Nassenstein, Z. Naturforsch 8A 90 (1953).

[7] T. A. Davis and K. Vedam, J. Appl. Phys. 38 4555 (1967).

[8] R. W. Dixon, J. Appl. Phys. 38 5149 (1967).

[9] W. T. Mahoney and H. R. Carleton, IEEE Transactions on Sonics and Ultrasonics, SU 14 135 (1967).

[10] B. M. Ashkinadze et al., Soviet Phys.-Doc. 11 703 (1967).

[11] I. H. Malitson, J. Opt. Soc. Amer. 52 1377 (1962).

[12] M. J. Dodge, I. H. Malitson and A. I. Mahan, Appl. Optics 8 1703 (1969).

4.4.1.2. Liquid-Liquid Phase Separation in a Laser Glass*

J. H. Simmons and W. Haller

Inorganic Materials Division
Institute for Materials Research

A study underway at the National Bureau of Standards has involved measurements on various glass compositions to detect the possible presence of liquid-liquid phase transitions. This information is desirable as part of a laser damage study. It was found that a liquid-liquid phase transition occurs in a lithium-silicate glass, very similar to one in use as a laser glass, of the composition:

---

* An associated project, supported by the National Bureau of Standards.

SiO_2	66.1% weight
Li_2O	15.5%
CaO	10.1%
Al_2O_3	4.4%
CeO_2	0.5%
Nd_2O_3	3.2%

This glass composition has a consolute temperature between 441°C and 448°C, a temperature range close to its annealing point (approx. 460°C). Such results imply that a degree of microstructure will appear in the glass when it is heat-treated at temperatures below and around 440°C. The degree and size of the microstructure will then increase with the length of heat treatment. Since the consolute temperature occurs in the transformation region of this glass, a large degree of phase separation may (is likely to) occur during annealing.

4.4.1.3. An X-ray Transmission Method for Examining Ruby Laser Rods

E. N. Farabaugh and F. A. Mauer

Inorganic Materials Division
Institute for Materials Research

Objective

This study was undertaken to determine whether x-ray diffraction techniques may be used to characterize ruby laser rods. A correlation between crystal perfection and laser performance is being considered.

Approach and Results

Work has continued on the correlation of laser crystal perfection, as determined by x-ray diffraction techniques, and laser performance.

Since the last reporting period another group of laser rods has been examined using a modified high voltage transmission technique developed during this reporting period. The general features are shown in Figure 1. A slit, 11mm by 1mm has been placed a distance of 10cm from the x-ray source and the film placed parallel to the x-ray beam.

Pictures are taken at several points along the length of each rod. The beam samples a disc-shaped volume of the rod and produces an array of diffraction spots each of which is a crude x-ray topograph of the cross section (fig. 2).

The most recently examined group of three ruby laser rods was again obtained from Dr. J. Hall (NBS, Boulder). These rods all have better laser performance than the first group. Rod D, .330 in. in diameter by 3.0 in. long with rod axis parallel to <0110>, has residual strain and is described as "definitely inferior to rods E and F" by Hall. Rod E, 3/8 in. in diameter by 1 1/2 in. long with its axis parallel to <0110>, was described by Hall as being the best rod for laser performance that he has seen. Rod F, a 60° rod .620 in. in diameter by 3 11/16 in. long, was described as typical of the best available currently. This rod has some tracking damage. All rods are still capable of the laser performance described above.

Figure 3 is a composite of corresponding spots from five films taken along the length of rod D. These topographs show how the crystal perfection of the rod varies along its length. The best volumes of the rod are represented by those images of the cross section which are free of distortion and have a minimum of splitting. A wide range of crystal perfection is indicated by these films. Rod D was described by Hall as having some strain present which affected its angular distribution pattern. The topographic method used is not sensitive to strain and the films do not indicate this characteristic of the rod.

Figure 4 is a composite of corresponding spots from five films taken along the length of rod E, the "best" laser rod. These films also indicate a range of crystal perfection along the length of the rod. When this rod was examined under crossed polarizers, it was observed that it did not exhibit extinction uniformly across its cross sectional area (Hall was aware of this before sending the rod to us). The subgrains in the rod appear to run from end to end and are fairly regular. Thus, it is evident that a ruby rod can have very good laser performance and still not be very good crystallographically. In comparing the films of rods D and E it is seen that films are in general very similar, however, the laser performance of rod E is superior to that of rod D.

Films were also taken along rod F. None of these films are pictured because the images formed were very weak. The faintness of the diffraction images is due to the fact that

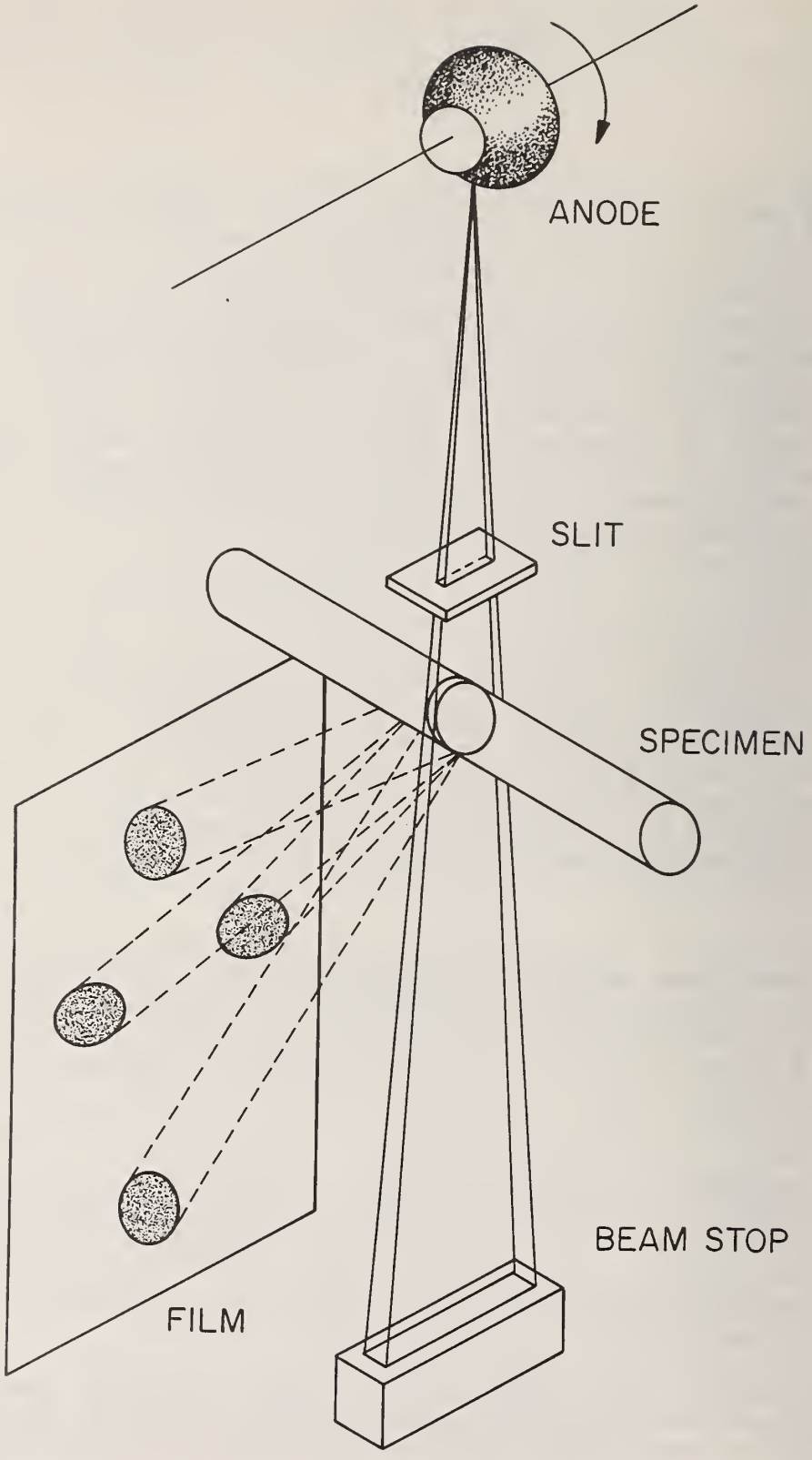

Fig 1. Modification of the Laue transmission technique to give a topograph of the cross section of the rods.

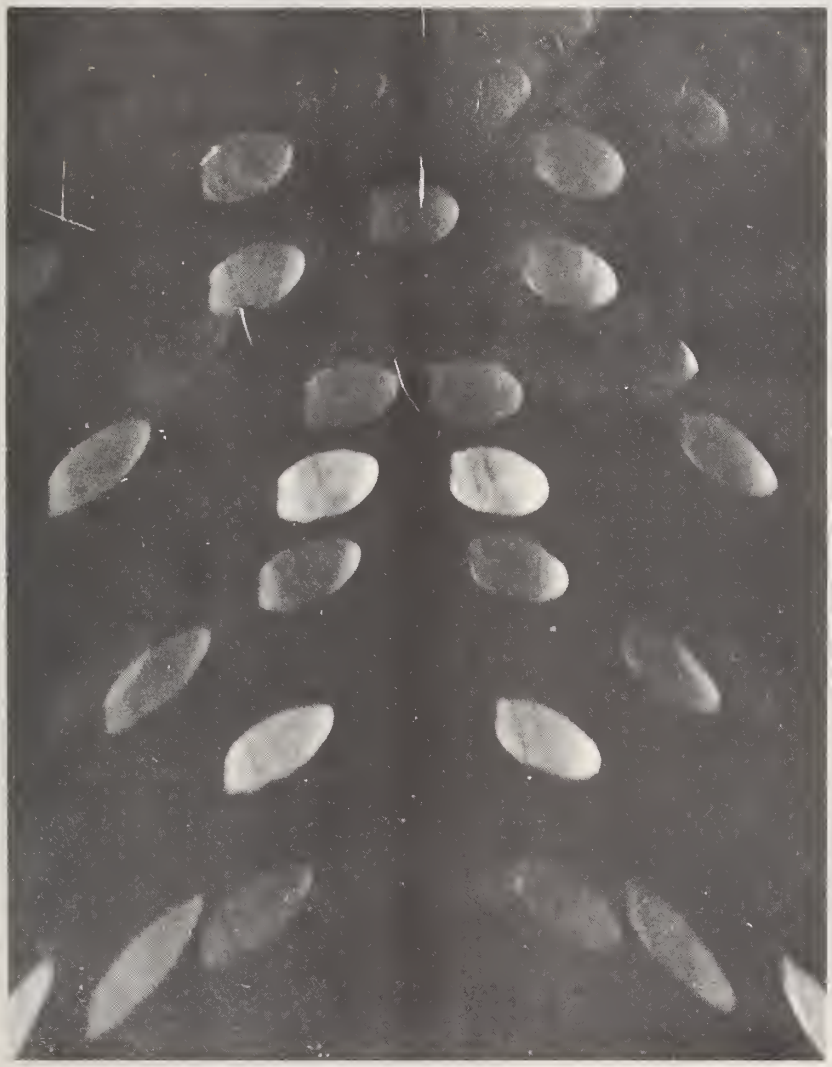

Fig. 2. Diffraction pattern of a ruby rod in which each spot is a crude topograph.

Fig. 3. Composite of corresponding spots from five films like the one shown in Fig. 2 taken along the length of rod D.

Fig. 4. Composite of corresponding spots from five films taken along the length of rod E.

in this rod we are approaching the limiting thickness of ruby rod that we can get an x-ray beam through. Inspection of these films showed spots which were well formed in every film with a minimum of splitting and distortion. Since all of the films were of the same quality we would evaluate this rod as better crystallographically than rod E. The laser performance is however, inferior to that of rod E. Rod F was described as possessing some tracking damage. Although our images are weak and not many spots appear, there is no evidence for this damage observable in the images.

The rods studied in the previous reporting period were re-examined using the new technique of topographing whole cross sectional areas. The results were in good agreement with the previous results and the performance could be correlated with the crystal perfection.

A badly damaged rod with bubbles, visible to the eye, was also examined with the modified transmission technique. The images formed gave no obvious indication that the bubble defects were present.

It has been demonstrated that the modified transmission Laue technique can detect misorientations in large single crystals. However, topographs of the cross section of the rods do not seem to be sensitive to defects other than grain boundaries, which are easily demonstrated. The first set of rods examined showed a correlation between the laser performance and crystal perfection. There was no similar correlation found with the second set of rods.

A possible different view of the problem which might be more fruitful is not to determine how many imperfections are shown in the topographs but to try to determine what are the features in the topographs we obtain which are important in the grading of the crystals for laser applications.

4.4.2. Damage to Laser Materials

4.4.2.1. Laser-Induced Damage Studies

N.N. Winogradoff, A. H. Neill, Jr., and J. Mitchell
in collaboration with:
W. Haller, G. Cleek and R. Waxler

Inorganic Materials Division
Institute for Materials Research

Objective

This was to set up a well defined laser glass damage facility for evaluating the damage threshold for various

samples of glass and elucidating the mechanisms responsible for the damage.

Approach

On establishing the facility, it will be used to, (1) measure the damage thresholds for various samples of glass, (2) catalog the different types of damage observed, (3) correlate the nature of the damage with the conditions under which the damage occurred and with the composition and heat treatment, etc. of the glass sample, and, (4) elucidate the mechanisms responsible for each type of damage.

Status

A "one gigawatt" neodymium laser system, capable of producing 20 ns. Q-switched pulses with energies in excess of 30 joules per pulse has been ordered and delivered.

The system consists of an oscillator, Q-switched by means of a Pockel's cell, feeding into two successive amplifier rods, and is currently undergoing acceptance tests.

Pending the operation of the above system, preliminary experiments on the damage of silica and glass samples by exposure to 3 joules, Q-switched, ruby laser pulses were undertaken.

Introduction

Bulk physical properties of glass samples indicated that the threshold for mechanical fracture decreased substantially as the water content was increased. This suggested that the threshold for damage by laser pulses might also be a function of the water content of the glass.

Since samples of silica with two distinctly different water contents [as measured by infra-red absorption, Figures (1) and (2)] were available, the above investigation was centered on these samples.

Experimental Procedure

The damage threshold of each sample was determined by changing the radiant flux density photons per square centimeter per second incident on it by moving a thin plate of the sample along the axis of a convergent, pulsed, laser beam.

The latter was generated by placing a biconvex lens with a focal length of 32 cms in close proximity to

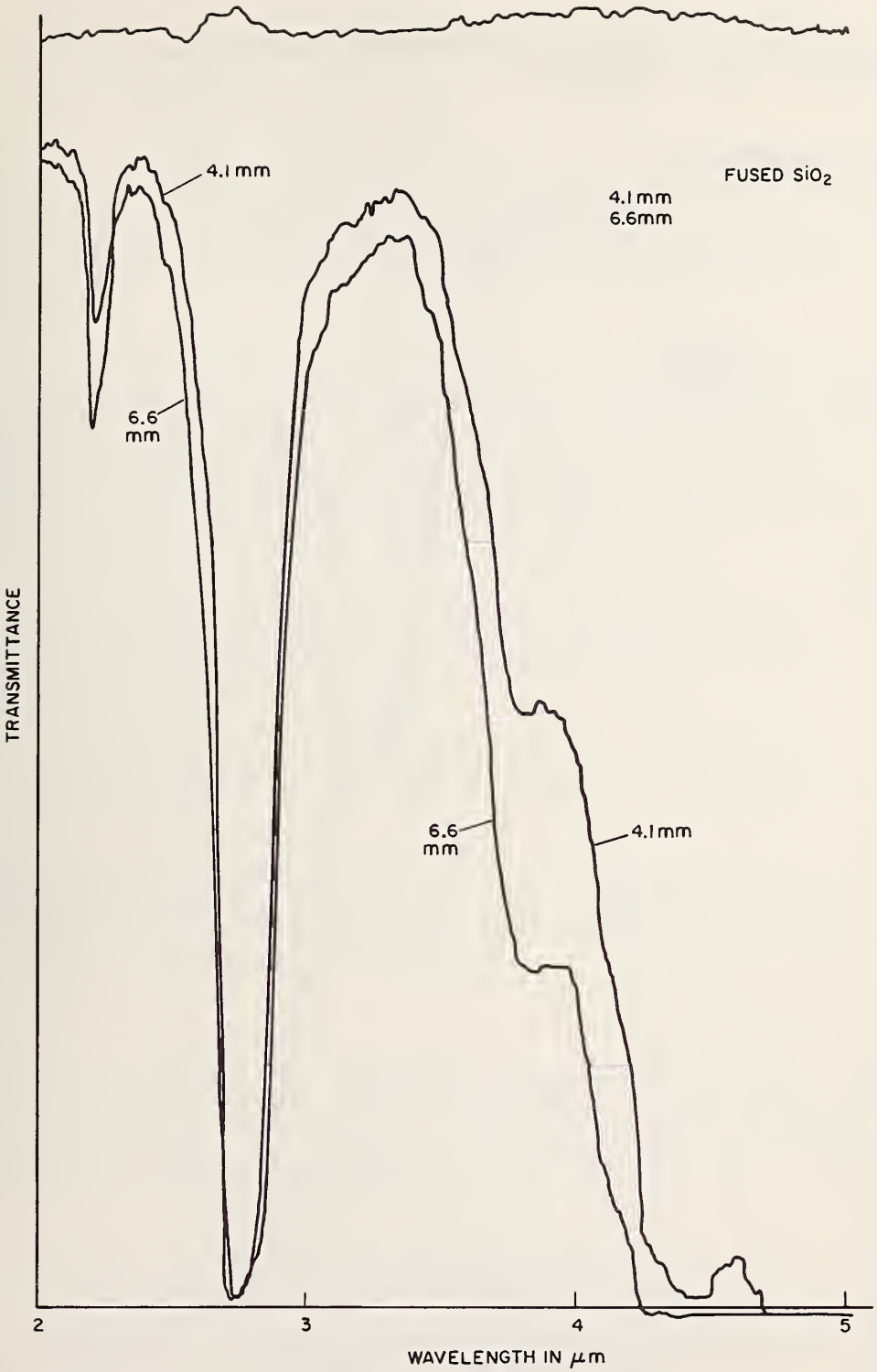

Figure 1. Infrared transmission of the two samples of high water content silica. Note the severe extinction at 2.7 μm indicating the presence of water. (G. W. Cleek)

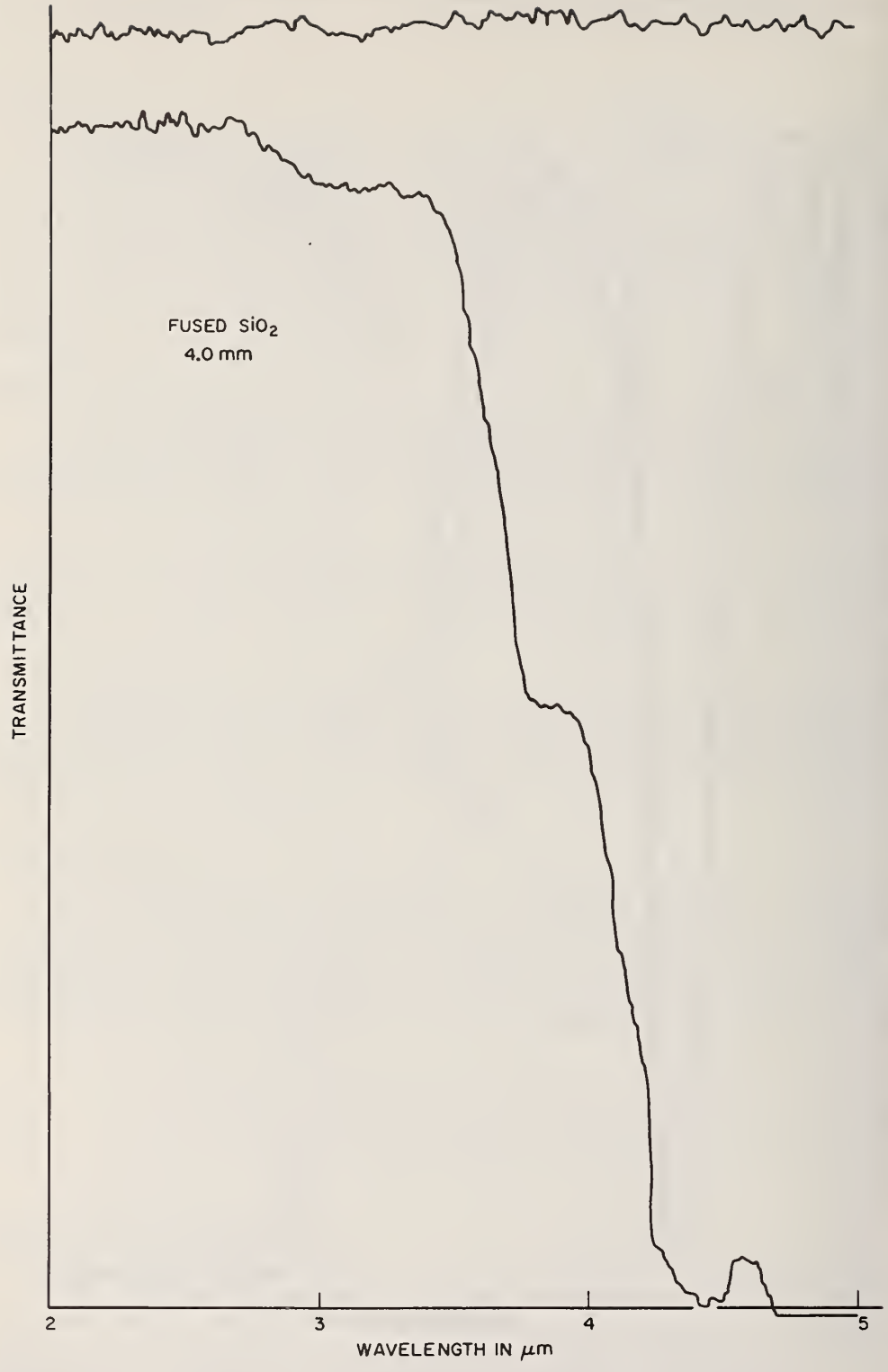

Figure 2. Infrared transmission of low water content silica. Note the absence of the water absorption band at 2.7 μm indicating that this sample had a very low water content.

the ruby laser. The radius of the beam emerging from the lens was measured at several points along the beam axis by its "printing" effect on black pvc adhesive tape. The resulting beam profile was as shown in Figure (3).

While it was recognized that this way of defining the beam profile was limited by the threshold for the printing effect, it proved to be fast and reproducible so that the data could easily be reduced to the low power peripheral contours which would be observable with a suitable photo-detector.

The total energy in a single pulse emerging from the lens was measured with a calibrated solid state calorimeter placed near the lens. The resulting measurement was correlated with the signal generated by an ITT bi-planar photo diode having an S1 spectral response, reacting to a fraction of the light beam reflected from a glass plate acting as a beam splitter as shown in Figure (4).

The correlation was carried out by using 10 successive shots, and these measurements showed that an ITT photo detector signal of 250 ±17 volts corresponded to pulsed beam energies of 1.5 ±0.1 joules.

The ITT detector was therefore used as a sensitive monitor for each flash of the laser used in our damage studies.

In measuring damage thresholds, the laser controls were adjusted so as to keep the monitor signals to within 250 ±17 volts and results obtained with monitor signals outside of that range were discarded.

Results

Neglecting refractive index and absorption effects, the results of our measurements and the damage threshold for silica samples with high and low water contents, together with that for a sample of Calcium Aluminate F75 are summarized in Table 1 and showed that:

(1) All the damage observed was restricted to the surface and was in the form of surface pitting.

(2) The onset of damage was accompanied by an acoustical signal and a flash of "white" light.

(3) Different samples, cut from the same slug gave damage thresholds which were reproducible to within 2.5 $J/cm^2/30$ ns.

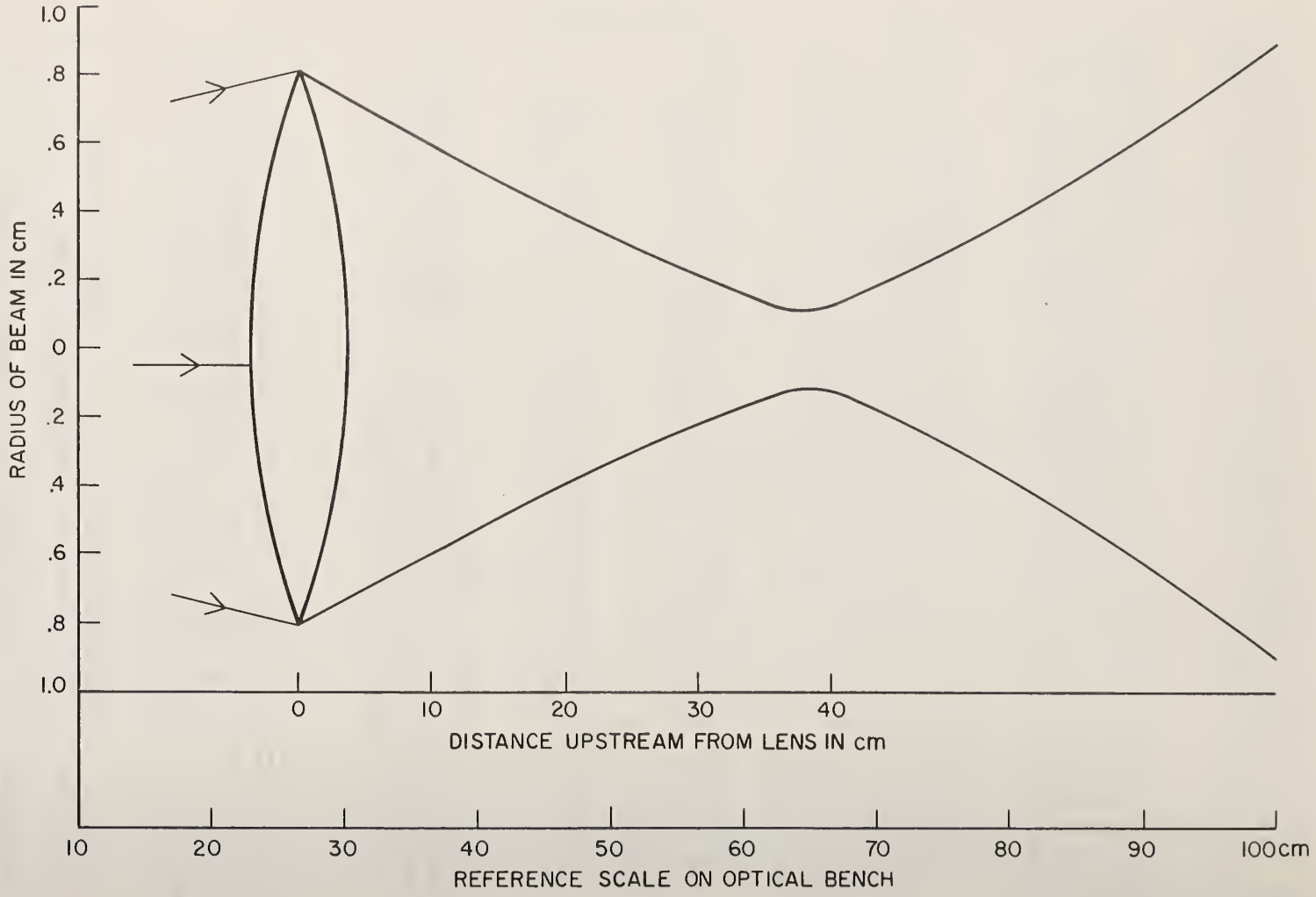

Figure 3. Curves defining the beam profile along the optic axis with reference to a meter stick. The energy/cm^2/30 ns falling on the surface of a sample placed perpendicular to the beam axis was determined from the position of of the surface relative to the meter stick.

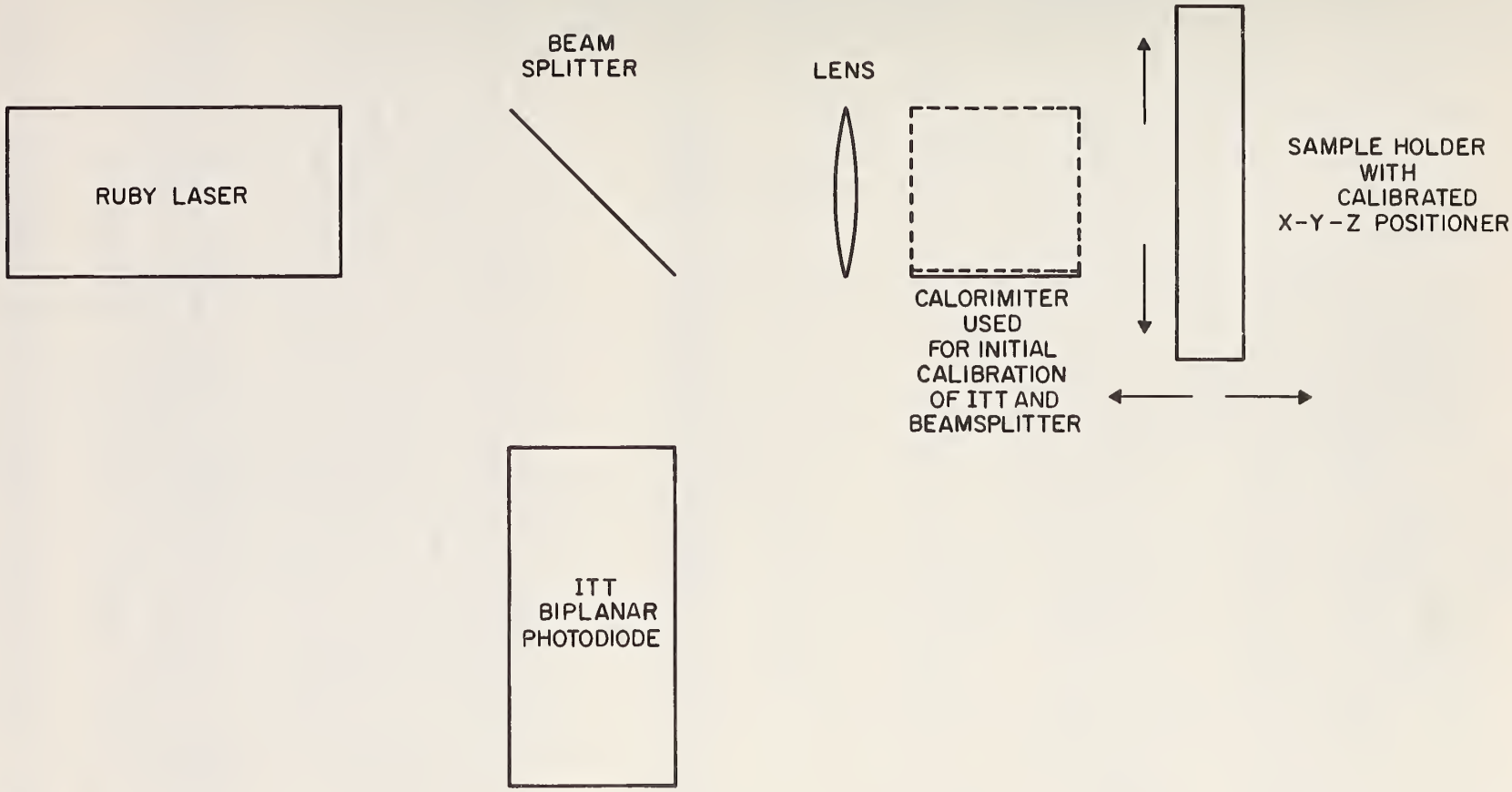

Figure 4. General plan of the apparatus used, showing relative positions of the laser head, beam splitter, ITT monitor and focusing lens.

TABLE 1

Sample	Position at which damage could be detected	Monitor Signal (Volts)	Damage Threshold 30 ns. pulses j/cm^2
High Water Content, Silica Sample Source(1)	57.9	208	11.3
High Water Content, Silica Sample Source(2)	63.5	198	25.3
Low Water Content, Silica	55.5	205	8.5
Calcium Aluminate	61.3	210	17.5

(4) Silica samples with the higher water content yielded a higher damage threshold than those having a lower water content.

Discussion

Samples of high water content silica derived from sources 1 and 2, of allegedly identical material showed very different damage thresholds, i.e. 12.5 and 26.5 J/cm^2 for 30 ns pulses. These two sets of samples could have had different surface polishing treatments and they were therefore both re-ground and re-polished by identical processes to ensure identical surface characteristics. However, the re-polished samples still showed the above difference in damage threshold, the cause of which is not understood.

Another factor of considerable interest was that, even after re-grinding and re-polishing, the high water content samples invariably damaged on the back surface where the energy density would be expected to be larger, while the low water content silica samples invariably damaged on the upstream surface.

The reason for this difference is not understood, and may be related to absorption effects in the samples.

Conclusions

Samples cut from one slug of silica containing a considerable amount of water (as indicated by Cleek's infrared absorption data of figure 1) indicated that the sample with the higher water content had a higher threshold for damage for 30 ns. pulses, 25 J/cm^2 versus 8 J/cm^2 respectively. This conclusion is rendered less certain by the fact that samples from the other slug of silica also known to contain a similar amount of water, had a damage threshold of only 11.8 J/cm^2 for the 30 ns. pulses.

It appears that factors other than water content play a major part in determining the damage threshold. Assuming that the two compositions can be regarded as being the same, it appears that the heating and cooling conditions used in the fabrication may have been different and may have a strong effect on the damage threshold.

Definite knowledge of the sample's total history is therefore essential for understanding the results of damage experiments.

4.4.2.2. Inclusions in Laser Materials*

Herbert S. Bennett

Inorganic Materials Division
Institute for Materials Research

Objective

One of the severe problems encountered in high power laser systems is the internal damage of the laser and its optical elements. One type of internal damage arises from metallic or dielectric inclusions. The present study examines the feasibility of using optical techniques to detect such inclusions before they cause damage. Detecting an inclusion before it causes damage eases the burden of the chemical analysis near the incipient damage area. During this report period, attempts have been made (1) experimentally to detect incipient damage centers by light scattering techniques, and (2) theoretically to evaluate the prospects of detecting such centers by the thermal disturbance created in the glass around them when subject to a laser pulse having an energy below the damage threshold energy.

---

* An associated project, supported by the National Bureau of Standards.

Light Scattering Experiments

Azimuthal and forward light scattering techniques have been suggested as possible ways to detect such centers. Two Nd-glass rods (Owens-Illinois ED-2, 2.54 cm in diameter by 5.08 cm in length) have been examined in such light scattering experiments at NBS and at the Air Force Cambridge Research Laboratories. The object is to see whether differences between the two rods can be detected by scattering methods which do not rely upon the human eye and yet provide an examination of essentially the whole rod. The search and seek ability of the human eye is very advantageous when compared with the limitations of such devices as photo multiplier tubes and photo-diodes. One sample was rated excellent and the other sample was rated as less than excellent but not poor either. The ratings were given by H. A. Lee of Owens-Illinois.

The azimuthal light scattering measurements were performed at NBS and were reported in NBS Technical Note Number 514. These measurements indicated that the forward scattering might be more fruitful. Dr. Martin Stickley and Mr. Edmund Hoell agreed to perform small angle scattering measurements on the above two samples. Their results were communicated to NBS in the form of a letter. A copy of the letter and data is given with their permission in the appendix to this project report. We thank them very much for their cooperation and for their efforts in measuring the small angle scattering. Even though they can distinguish rod A from rod B, the difference is marginal for the detection of a small number of inclusions which are less than tens of microns in size. The technique does not seem feasible as a way to maintain quality control for inclusions leading to damage. The technique does have promise for detecting striae however.

Theoretical Treatment of Laser-Induced Thermal Disturbance Near Inclusions

The heat diffusion equation with time dependent boundary conditions is solved for the temperature as a function of position and time. The optical path length change for a light ray passing near the inclusion, the radial and tangential components of the stress tensor, and the radial and tangential changes of the local index of refraction due to the thermal stress field are computed from a knowledge of the space and time variations of the temperature.

Results

The initial computations apply to two cases of prime practical interest. These are platinum spheres in a laser glass host.

Case 1. A 30 nsec. laser pulse with an energy density of 30 (J/cm^2) encounters a platinum sphere of radius .01 cm.

Case 2. A 30 nsec. laser pulse with an energy density of 3 (J/cm^2) encounters a platinum sphere of radius .001 cm.

Because the model assumes that strain is proportional to stress the energy density of the laser pulse has been so far limited to values such that the temperature of the glass never exceeds the strain point of glass. Laser glasses have strain points around 600°C. This is the reason why the energy density is less for Case 2 than it is for Case 1.

The theoretical model predicts for Case 1, that the largest optical path length changes are about 5×10^{-6}cm and occur for a range of distances of closest approach to the platinum sphere from .01 cm to .03 cm. The time interval during which the path length changes are large is from .03 seconds to .3 seconds after the beginning of the 30 nanosecond pulse. The tangential and radial stress components have magnitudes which do not exceed 10^{10} ($dynes/cm^2$). Maximum stress occurs at the end of the laser pulse and is a factor of 10 less than the bulk moduli of the laser glass. The magnitudes of the radial and tangential changes of the index of refraction due to thermal stress birefringence do not exceed 10^{-3}. These values of the stress birefringence obtained for the same values of radial distance and time as those for the optical path length changes. The maximum temperature occurs at the end of the laser pulse and is 618°C at the surface of the particle. The maximum radial rate of expansion of the platinum sphere is 2×10^3 (cm/sec). This expansion occurs during the laser pulse and its rate is about a factor of 100 less than the speed of sound in laser glass.

The theoretical model predicts for Case 2, that the largest optical path length changes are about 2×10^{-9} cm and occur for a range of distances of closest approach to the platinum sphere from .001 cm to .01 cm. The time interval during which the optical path length changes are large is much smaller than that for Case 1. The maximum path length changes occur at about .03 sec. At .003 sec., the path length changes are less than 10^{-14} cm and at .3 sec. they

are less than 10^{-25} cm. The magnitudes of the tangential and radial stress components do not exceed 10^{10} (dynes/cm^2). The maximum stress occurs at the end of the laser pulse and is a factor of 10 less than the bulk moduli of the laser glass. The magnitudes of the radial and tangential changes of the index of refraction due to thermal stress birefringence do not exceed 10^{-3}. The latter values are greatest for the same values of radial distance and time as those for the maximum optical path length change. The maximum temperature at the interface between the platinum and the glass is 611°C and occurs at the end of the laser pulse. The maximum value of expansion of the platinum sphere occurs during the laser pulse and is about a factor of 1,000 less than the speed of sound in glass.

Conclusions

The above calculations suggest two possible methods by which incipient absorbing centers might be detected. One method would use the interference of two light rays which experience different optical path length changes and the other method would use thermal stress birefringence. Because optical path length changes greater than one tenth the wavelength of the probing light are required to produce detectable fringe shifts, case 1 and case 2 indicate marginal feasibility for either of the above methods. However, calculations such as case 1 and case 2 and preliminary additional calculations, which apply to millisecond pulse widths but are not reported here, suggest the direction in which one should go to optimize the optical path length changes without causing damage. Heating the inclusion over a longer period of time to the same surface temperature of about 600°C gives greater spatial extents to the changes in indices of refraction. Another approach is to employ pulse widths and observation times which are less than the relaxation times of the host. Relaxation times for laser glasses between 800°C and 1100°C are approximately between nanoseconds and microseconds. These are estimates of the time during which stress is proportional to strain in glasses which are not elastic for infinite time. Such short time observations will permit one to raise the inclusion surface temperature substantially above the present 600°C reported here and still satisfy the assumptions of the present model. The author plans to extend his calculations to longer pulse widths and to higher temperatures.

Most of the other optical methods that have been suggested are capable of examining only small volumes at any one time and additional scanning methods are essential if an entire sample is to be studied. For example, K. Vedam

et al., J. Appl. Phys. 37, 2551 (1966), report ultramicroscopic techniques by which they illuminate a 20μ thick layer and by which they can detect 0.35μ particles with a (1/32) sec exposure for the camera. They also have estimated that 0.03μ particles might be detected with one hour exposure. The major disadvantage is that the layer under observation must be less than about 2 cm from the surface of the sample. Researchers should be able to examine much larger volumes of the sample by the techniques considered in this report.

The above computations suggest that examining incipient absorbing centers in laser glasses by methods which employ thermal stress birefringence are more promising than methods which use the interference of two light rays which experience different optical path length changes due to the local variation of the index of refraction near the platinum sphere. However, because the propagation of light in the presence of a stress birefringence which has spherical symmetry is complex, the interpretation of the birefringence data will be more tedious than the interpretation of data from an interference method.

Additional computations suggest that the use of laser pulses with pulse widths of the order of milliseconds may be more promising for the detection of small incipient absorbing centers. The longer pulses produce changes in the index of refraction which extend over greater distances.

The present theoretical model can be applied to any spherical inclusion which has a thermal conductivity greater than that of the host. For example, antimony inclusions. which have been detected in some laser glasses, can be treated readily within the framework of the present model. Applying the present model to this and other cases is planned. In addition, attempts will be made to remove some assumptions contained in the present model in order to make it applicable to a wider class of problems. Some researchers suggest that metallic inclusions at very high temperatures may have thermal conductivities comparable to that of the host. For this reason, it would be most useful to remove the restriction that the thermal conductivity of the inclusion be greater than that of the host. Computationally feasible solutions do not exist at present for this more general case; but additional efforts to this end might prove successful. Also, the degree of thermal contact between an inclusion and the host should be examined during and after the laser pulse. It is certain that the state of thermal contact at the initiation of the laser pulse depends upon the past thermal history of the

host. Finally, any comprehensive study of inclusions in laser materials should at least attempt to answer the difficult question of how do the thermal properties and elastic properties of the inclusion and host change during and after the laser pulse. Workers in this area should be aware of this last question, but rigorous answers are not likely to be given in the immediate future. It is for this reason that such theoretical models as the above can at best serve only to guide the experimental researchers on the damage problem.

Method

The author shall outline below the model upon which the above calculations were based. He considers an absorbing sphere of radius r_o imbedded in a host of infinite extent. The thermal properties are the density ρ (gm/cm^3), the specific heat C (J/gm°C), and the thermal conductivity K (J/cm sec°C). The derived thermal quantities of thermal diffusivity $a^2 = (K/\rho C)$ and the volume specific heat $h = \rho C$ also enter the calculations. The subscript c on any of these thermal properties will refer to the absorbing center and the subscript h will refer to the host.

The diffusion equation describes the time and space dependence of the temperature $T(\underset{\sim}{r},t)$ for large distances $\underset{\sim}{r}$ and for large times t.

$$\frac{\partial T(\underset{\sim}{r},t)}{\partial t} = a^2 \nabla^2 T(\underset{\sim}{r},t) \qquad (1)$$

where ∇^2 is the Laplacian operator. The diffusion equation is valid only when local thermal dynamic equilibrium exists. It becomes suspect for distances comparable to atomic dimensions and for times comparable to the phonon-phonon collision time. A typical phonon-phonon collision time at room temperature is 10^{-11} sec. Hence its validity for nanosecond laser pulses is certainly more justified than for picosecond laser pulses. The diffusion equation requires a statement of initial conditions and boundary conditions before a solution is uniquely defined. The initial condition is that the

$$T(\underset{\sim}{r},t) = \begin{cases} 0 & t \leq 0 \\ T(\underset{\sim}{r},t) & t > 0 \end{cases} \qquad (2)$$

The boundary conditions are time dependent for any realistic treatment of the problem. The temperature must be finite everywhere, $T(\underset{\sim}{r}=\infty,t)$ = finite and $T(\underset{\sim}{r}=0,t)$ = finite. The continuity of the temperature across the center-host interface is

$$T_c(\underset{\sim}{r}=r_o\hat{r},t) = T_h(\underset{\sim}{r}=r_o\hat{r},t).$$

The host is assumed to be very transparent to the laser energy and absorbs only a negligible amount of energy from the laser beam. The conservation of heat flow at the interface gives

$$-K_h\underset{\sim}{\nabla}T_h(\underset{\sim}{r}=r_o\hat{r},t)\cdot\hat{r} = -K_c\underset{\sim}{\nabla}T_c(\underset{\sim}{r}=r_o\hat{r},t)\cdot\hat{r}+H(t)\hat{z}\cdot\hat{r}, \qquad (3)$$

where $\hat{r}$ is the unit radial vector and $\hat{z}$ is the unit vector in the z direction. The heat flux H(t) the heat absorbed by the sphere from the laser beam.

$$H(t) = \begin{cases} Q & 0 \leq t \leq \tau \\ 0 & t>\tau \text{ and } t<0 \end{cases} \qquad (4)$$

The radiation of heat by the interface and by the glass close to the sphere is not included in this model. A black-body at 600°C produces a heat flux of .735 (J/sec cm^2). The laser beam for Case 1 contains a heat flux of 10^9 (J/sec cm^2). The temperature gradients which occur from the time of cessation of the laser pulse to the time of maximum optical path length change are always sufficiently large so that $|K_h\underset{\sim}{\nabla}T_h|$ is greater than the heat flux due to the radiation. Of course, the heat flux $-K_h \cdot \underset{\sim}{\nabla}T_h$ becomes small for times greater than a second and the radiation effects should be studied in both the diffusion equation and in the boundary conditions. Because the temperature is close to the ambient temperature whenever the time is greater than a second the long time behavior is not in the region of practical interest for detecting incipient centers before they cause damage.

Because $a_c^{-2} \approx .025\ a_h^{-2}$ and $K_c \approx 92\ K_h$ the temperature gradients in an absorbing center such as platinum would

be much less than those for the glass host. In the limit of $K_c >> K_h$, Equation (3) simplifies to give a spherically symmetric problem:

$$-K_h \frac{dT_h(\underset{\sim}{r}=r_o\hat{\underset{\sim}{r}},t)}{dr} = \frac{H(t)}{4} - \frac{\rho_c C_c}{3r_o} \frac{dT_c(\underset{\sim}{r}=r_o\hat{\underset{\sim}{r}},t)}{dt} \qquad (3')$$

The solution for the temperature is obtained by taking the Laplace transform of the diffusion equation, the initial condition, and the time dependent boundary conditions. The transformed equations become linear equations for the Laplace transform $U(\underset{\sim}{r},S)$ of the temperature $T(\underset{\sim}{r},t)$. The analytic properties of the Laplace transform $U(\underset{\sim}{r},S)$ for complex values of S gives rise to three distinct types of behavior for $T(\underset{\sim}{r},t)$. The volume specific heat ratio ($R = 4h_c/3h_h$) determines the three regions of behavior; namely $R < 1$, $R \equiv 1$, and $R > 1$. This ratio is about 2.97 for platinum in laser glasses. For this case the function $1/U(\underset{\sim}{r},S)$ has zeros at two complex values of $\sqrt{S}=a\pm ib$. The Bromwich contour integral is evaluated to give the temperature $T(\underset{\sim}{r},t)$ from a knowledge of $U(\underset{\sim}{r},S)$.

Having thus obtained the temperature $T(\underset{\sim}{r},t)$ one may compute all the other quantities discussed above. The optical path length change ΔL becomes

$$\Delta L = \int_L (dn/dT)\ T(r,t)\ dx, \qquad (5)$$

where the integration is along a ray that has a distance of closest approach r_1 to the absorbing center and the variation of the index of refraction with temperature is (dn/dT).

The calculation of the stress components require a few more assumptions. The stress components satisfy second order differential equations in position for a given time and hence two coefficients must be determined. The boundary condition that all stress components vanish at distances infinitely far from the absorbing center determines one of the two coefficients. There are three possible sets of additional interface boundary conditions from which the second coefficient may be evaluated. The author has chosen to employ a slippery boundary at $\underset{\sim}{r} = r_o\hat{\underset{\sim}{r}}$. A slippery boundary obtains when the conditions listed below are valid:

a. The hydrostatic pressure in the absorbing center at $\underset{\sim}{r} = r_o\hat{r}$ equals the radial stress component in the host at $\underset{\sim}{r} = r_o\hat{r}$.

b. The tangential stress components are discontinuous across the boundary at $\underset{\sim}{r} = r_o\hat{r}$.

Given conditions a and b, one uses the poisson ratio and the Young's modulus for the host and the isothermal compressibility of the absorbing center to compute the second coefficient. This second coefficient and the temperature $T(\underset{\sim}{r},t)$ then yield the radial and tangential stress components and the radial rates of expansion and contraction of the absorbing center. From a knowledge of the stress components the stress birefringence may be computed. If the rates of expansion and contraction of the absorbing center approach the speed of sound in the host then the above problem becomes a nonlinear one involving two coupled differential equations. One equation treats heat diffusion and the other treats energy transfer in the form of sound or shock waves.

The author developed an extensive computer program to evaluate all quantities given in Cases 1 and 2 for all possible values of the ratio $0 < R < M$, where M may be large but finite.

Appendix

Small Angle Scattering from Nd-doped Laser Glass

Appendix 1 contains the letter and data communicated to NBS by Dr. Martin Stickley. This letter and data are referred to in the Section 1 of the project report entitled Inclusions in Laser Materials.

DEPARTMENT OF THE AIR FORCE
HEADQUARTERS AIR FORCE CAMBRIDGE RESEARCH LABORATORIES (OAR)
LAURENCE G. HANSCOM FIELD, BEDFORD, MASSACHUSETTS 01730

REPLY TO ATTN OF: CROL/C. M. Stickley/2694 23 December 1969

SUBJECT:

TO: Dr. Herbert Bennett
National Bureau of Standards
Washington, D. C. 20234

Dear Herb,

Enclosed are graphs of the scatter loss vs. full angle for Owens-Illinois Rods A and B. Also included is the data after reduction by use of the formula found on the glossy figure (AFCRL photo 109-344).

I think the system for measuring this scatter loss has been working as well as it ever will be; to do better than we have done would require a greater effort than I am willing to put into the project. For full angles greater than 0.35 milliradians the standard deviation turned out to be about 0.8% or less which when converted into a loss coefficient gives a standard deviation of about 0.001 cm^{-1}.

As you can see from the graph of the average for 10 runs on Rod B, the loss is extremely low. I do not know how much of this loss could be due to small angle surface scatter, thus it is included in these results. For the sake of computing a loss coefficient I did not attempt to subtract out a representative amount for it however. As you can see from the error bars, the loss is about zero, however the averages for the 10 readings were still on the positive side of zero for the largest angles (1.6 and 0.8 mrad) where the data is usually the most reliable. The uncertainty gets quite high at low angles (1.6×10^{-4} radians) probably because the intensity of the gas laser beam is highest right in the center, and any error in replacing the aperture will show up readily.

A comparison of rods A and B shows that the average transmission of Rod B is equal to or higher than that for Rod A in every case even though the error bars overlap. One factor that could cause this would be the optical quality of the samples. We did position the beam so that it went through the region of best quality of each rod, and to our eye they looked the same, but whether this measurement is more sensitive than our eye is unknown to me at the present time. Thus, if this factor is negligible, I would say Rod B is better than Rod A, but this difference is so slight that it is unimportant in the operation of the material as a laser. I am also enclosing photographs (positives and negatives) of the intensity distribution in the far field for both rods and for the case where no rod is present. The negatives can be used for making more prints if you so desire. The far field distribution is not what would be predicted theoretically since the illumination of the 4.2 mm aperture was Gaussian-like.

I am going to send Haynes Lee a copy of this letter plus attachments since I suspect he is interested in these results too. We would also be interested in finding out which of these rods is the better one. Ed Hoell, the person who made the measurements, thinks Rod B is and the data supports his feeling. Also, he is due credit for making these measurements. It is due to his persistence and conscienciousness that they came out as well as they did. I hope these results will be of use to you in your laser glass program.

Sincerely,

Martin S

C. MARTIN STICKLEY
Chief, Laser Physics Branch
Optical Physics Laboratory

cc: Haynes Lee
E. Hoell

Dielectric Rod Small Angle Scatter Measurement

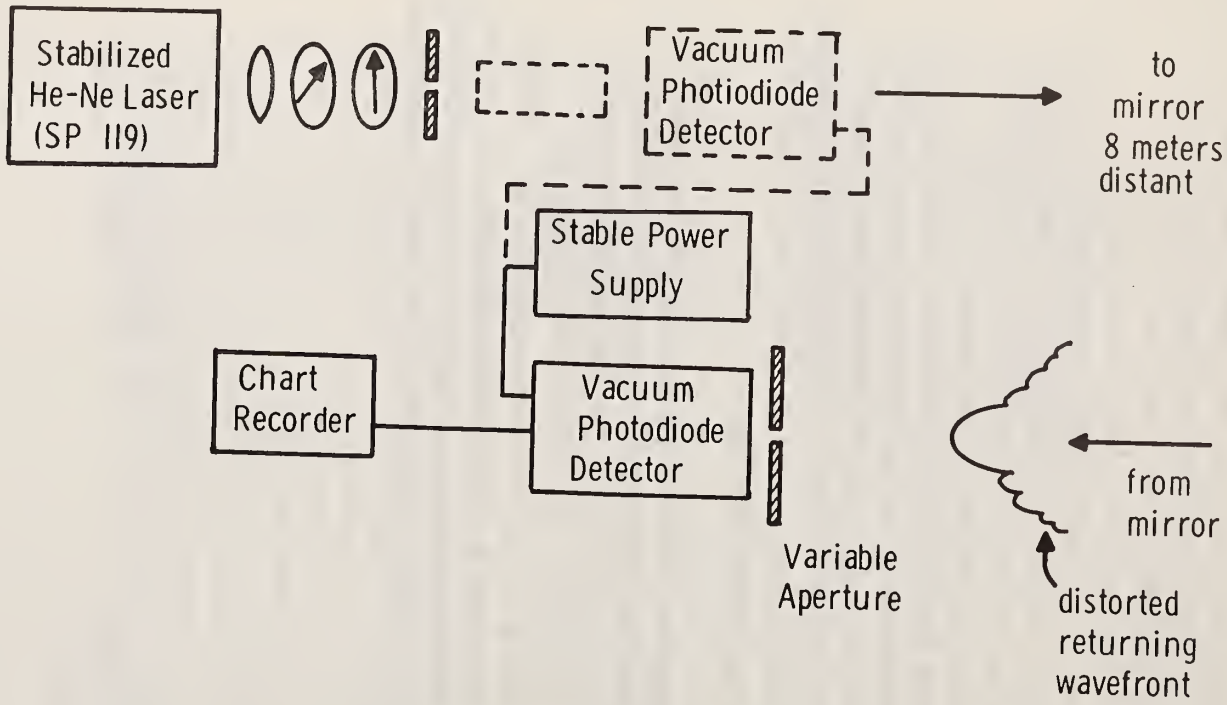

$$T = \frac{T_{\text{far field}}}{T_{\text{near field}}\ T_{\text{diffraction}}}$$

$$\text{Scatter loss} = \frac{1}{\ell} \ln\left(\frac{1}{T}\right) \; ; \qquad \ell = \text{laser rod length}$$

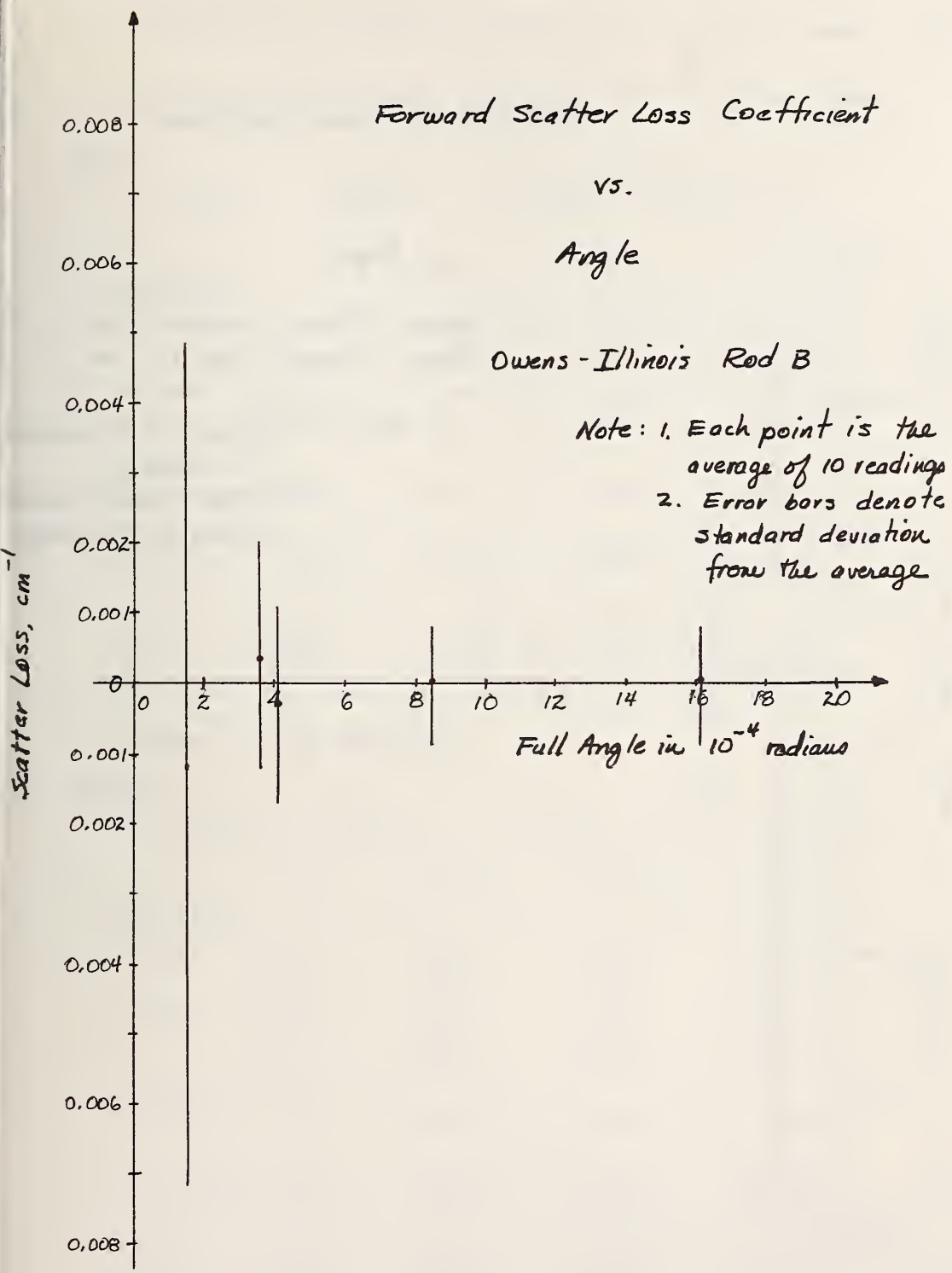
Forward Scatter Loss Coefficient
vs.
Angle
Owens-Illinois Rod B
Note: 1. Each point is the average of 10 readings
2. Error bars denote standard deviation from the average
Scatter Loss, cm⁻¹
0.008
0.006
0.004
0.002
0.001
0
0.001
0.002
0.004
0.006
0.008
0
2
4
6
8
10
12
14
16
18
20
Full Angle in 10⁻⁴ radians

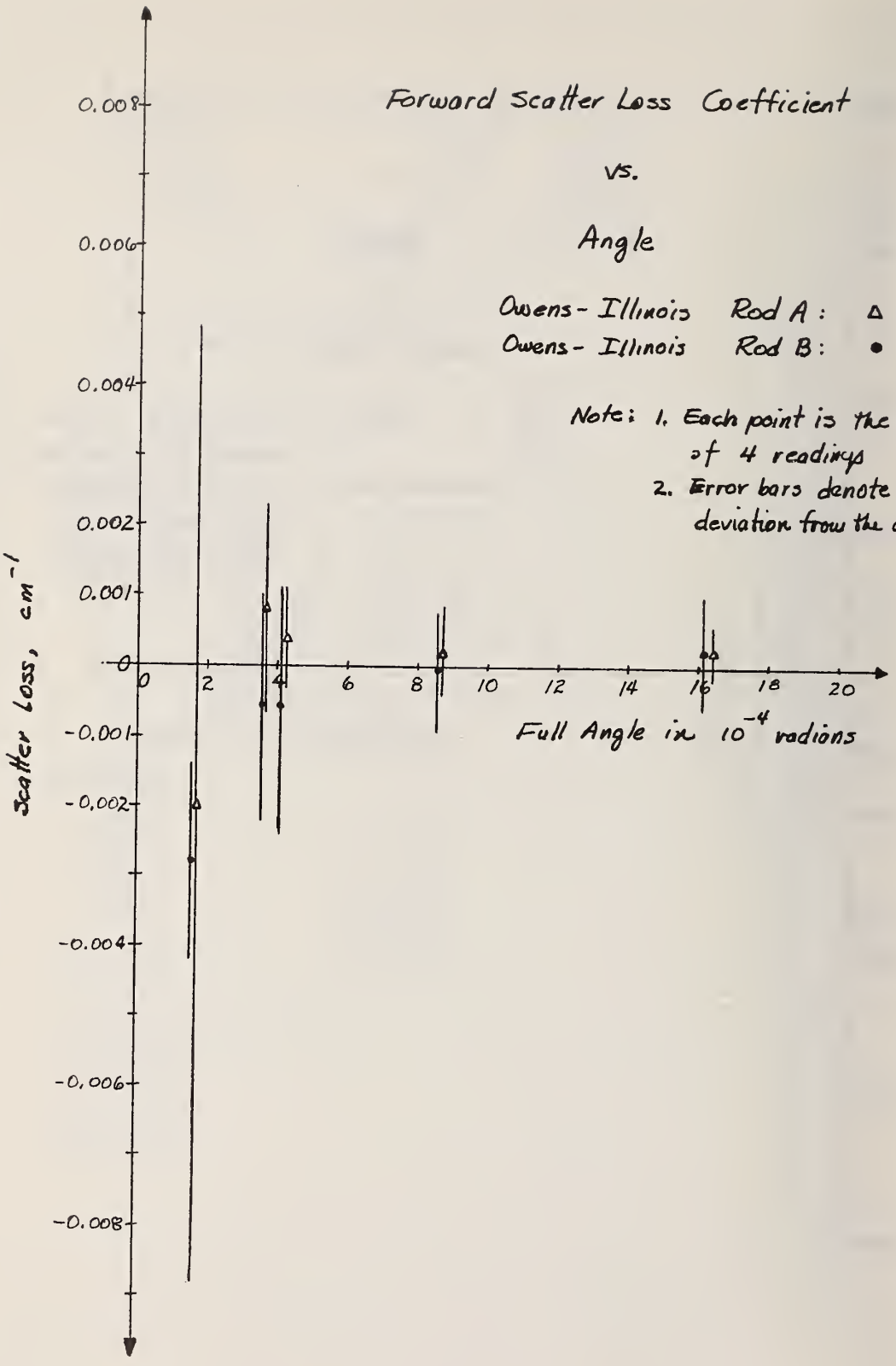
Forward Scatter Loss Coefficient
vs.
Angle
Owens-Illinois Rod A: △
Owens-Illinois Rod B: •
Note: 1. Each point is the average of 4 readings
2. Error bars denote standard deviation from the average
Scatter Loss, cm⁻¹
0.008
0.006
0.004
0.002
0.001
0
-0.001
-0.002
-0.004
-0.006
-0.008
0
2
4
6
8
10
12
14
16
18
20
Full Angle in 10⁻⁴ radians

DATA SUMMARY: FORWARD SCATTER LOSS OF O.I. Glass RODS

I. comparison of Owens Illinois Rods A & B; Lengths = 5cm

Rod A

Fractional Transmission vs. Angle (in millirodians)

Θ =	1.62	0.855	0.405	0.369	0.164
Date of Data					
12/11/69	1.000	0.996	0.997	0.987	0.977
"	0.996	1.001	0.996	0.991	1.006
12/12/69	0.999	0.996	1.004	1.004	0.982
"	1.001	1.003	0.994	1.003	1.074
Average Transmission	0.999	0.999	0.998	0.996	1.010
Standard Deviation	0.0019	0.0031	0.0038	0.0074	0.034
Scatter Loss, cm^{-1}	+0.0002 ± 0.0004	+0.0002 ± 0.0006	+0.0004 ± 0.0007	+0.0008 ± 0.0015	−0.0020 ± 0.0068

Rod B

Fractional Transmission vs. Angle (in millirodians)

Θ =	1.62	0.855	0.405	0.369	0.164
Date of Data					
12/11/69	1.001	1.000	1.004	1.004	1.023
"	0.994	0.999	0.994	1.000	0.996
12/12/69	1.004	1.007	1.016	1.015	1.065
"	0.997	0.996	0.997	0.993	0.971
Average Transmission	0.999	1.0005	1.003	1.003	1.014
Standard Deviation	0.0038	0.0040	0.0085	0.0080	0.0070
Scatter Loss, cm^{-1}	+0.0002 ± 0.0008	−0.0001 ± 0.0008	−0.0006 ± 0.0017	−0.0006 ± 0.0016	−0.0028 ± 0.0014

DATA SUMMARY : FORWARD SCATTER LOSS OF O.I. GLASS ROD

II Ten Run Average of Owens Illinois Rod B

Fractional Transmission vs. Angle (in milliradians)

θ =	1.62	0.855	0.405	0.369	0.164
Date of Data					
12/4/69	1.004	1.000	0.997	0.996	1.036
"	0.999	1.007	0.991	0.988	0.955
12/9/69	0.993	1.000	1.001	0.993	0.991
"	0.999	0.993	0.994	0.991	1.001
12/10/69	1.006	1.000	1.006	1.006	1.032
"	1.000	0.996	1.015	0.996	0.991
12/11/69	1.001	1.000	1.004	1.004	1.023
"	0.994	0.999	0.994	1.000	0.996
12/12/69	1.004	1.007	1.016	1.015	1.065
"	0.997	0.996	0.997	0.993	0.971
Average Transmission	0.9997	0.9998	1.0015	0.9982	1.0061
Standard Deviation	0.0041	0.0042	0.0071	0.0078	0.0290
Scatter Loss, cm^{-1}	$+0.00006 \pm 0.0008$	$+0.00004 \pm 0.0008$	-0.00030 ± 0.0014	$+0.00036 \pm 0.0016$	-0.0012 ± 0.006

4.4.3. Degradation of Laser Materials

4.4.3.1. Crystal Defect Studies on Laser Materials

R. F. Blunt, T. Chang, M. I. Cohen, and T. Tsang

Inorganic Materials Division
Institute for Materials Research

Objective

This investigation is a study of the causes responsible for degradation of performance of solid state lasers. The effort has been directed largely to a study of orange degradation of laser ruby, by EPR and optical means. (See NBS Technical Note 514 for previous report).

Technical Approach

Procedures followed are a continuation of those followed previously with the incorporation of appropriate additions and changes. Experimental measurements consist largely of optical absorption spectra and electron paramagnetic resonance on a variety of specially prepared "ruby" samples:

1. Detailed spectra taken on undamaged ruby is compared with corresponding spectra on "orange" degraded samples. These include specially prepared "ruby" as well as "laser quality" material.

2. Spectra will be examined for evidence of trace impurities, and, in the case of "orange" ruby, typical EPR crystal defect spectra that correlates with the orange coloring bands. This is of particular interest in view of the suggestion of Stickley, et al. [1] that discoloration may arise from color centers created by the pumping light at defects initially present in the crystals.

3. Special attention will be given to the detection of Cr^{4+} and/or Cr^{2+} ions that may exist in the orange samples. This effort includes a study of the $\Delta m = 2$, EPR transition reported by Hoskins and Soffer[2] and by Mason and Thorp. [3]

4. A number of doped sapphire crystals are grown and studied. Included are: rubies covering a wide range of Cr concentration; crystals containing other single metal impurities; and several "double doped" with Cr and one other metal.

5. Most crystals are colored by radiation with 50 KV x-rays, but recently ^{60}Co γ-irradiation has been occasionally employed.

6. Bleaching of the orange coloration by ultra-violet light and by H_2 plus heat in the case of the M_g doped rubies is conducted.

7. Coloration by laser pumping light and/or high power mercury arc sources is under way.

Experimental Results

With very few exceptions measurements were made on samples cut from Verneuil crystals grown in this laboratory. Metallic dopant concentration quoted are the nominal "starting material" values or, in the case of Cr, usually the value determined by the optical absorption method of Dodd, Wood, and Barns. [4]

The previous report describes the coloration produced by x-ray irradiation produced in both "in house" rubies and laser quality rubies. These several additional bands include, especially, a broad band centered near 0.47 μm and additional bands or long "tail" extending beyond 0.6 μm. Single doping of "pure" sapphire with various metals, principally transition elements, yielded x-ray coloration only in the ultra-violet.

Double doping with Cr and one additional metal, yielded, in the case of Cr plus Mg, an orange coloration at the time of growth. A careful choice of doping levels, viz. 0.025 mol% MgO and 0.0034 mol% Cr_2O_3 (i.e. 0.005 wt % Cr_2O_3) gave an orange coloration, apparently identical to that produced by x-rays. Further, it was shown that the coloration was far greater than that of the normal Cr^{3+} absorption spectra. The simple chemical picture of Mg^{2+} converting even all of the Cr^{3+} into Cr^{4+} would require very excessive oscillator strength for Cr^{4+}. Thus we concluded that the x-ray coloration is probably not directly caused by Cr^{4+} and is quite likely derived from some other mechanism, perhaps due to a trapped hole or electron model, i.e. a color center. The possibility of the oxidation of Cr^{3+} to Cr^{4+} still exists, and, of course, the presence of chromium is essential to the coloration.

Several experiments reported earlier have been repeated and extended. The possibility of defects being produced in sapphire by Cr plus Ti doping and by doping with Mg alone have been repeated using 50 KV x-ray irradiation. The original results were obtained, viz. Mg doping gives susceptability to coloration in the ultra-violet only. The Cr plus Ti doping results in coloration similar to that of Cr alone.

We have attempted the bleaching of x-ray colored rubies and find that the ultra-violet radiation from a 150 watt Hg arc very effectively and quickly bleaches out the orange color. The color is easily restored with x-rays. Semi-quantitative tests with appropriate filters to remove only the shorter wavelengths indicate that the bleaching is done principally by wavelengths shorter than 0.3 μm.

It is also found that x-ray induced color is easily and reversibly removed by heating in air. Various workers report various temperatures as effective. We arbitrarily chose 1400°C as certainly higher than necessary but still very low with respect to the 2050°C melting point. Thermal bleaching of a number of samples was done with the expected easy re-coloration.

Since the incorporation of Mg results in coloration by what would seem by elementary chemical arguments to be a simple oxidation of the Cr^{3+} to Cr^{4+}, the possibility of reduction and hence bleaching by heating in a hydrogen atmosphere must be considered. It was found that a 24 hour heating cycle in hydrogen at 1400°C results in bleaching, of the orange color of a Mg plus Cr doped sample, back to the normal Cr^{3+} pink color.

Heating in air restored the orange color. This apparent oxidation and reduction in the bulk sapphire at such a low temperature is not understood at this time and warrants further study.

As mentioned in the NBS Technical Note Number 514 (Progress Report for Project 300.0400 1 January to 30 June, 1969), we find that the x-ray coloration saturates with irradiation dosage, and reaches a saturation value for doses near 5×10^6 R/cm^2. In these discussions we consider only the prominent 0.47 μm band which we consider as typical. This is very typical of the often used "growth" curves employed in classical color center studies, and certainly suggests a model involving either crystal defects initially present or as we would prefer, mechanisms (defects or otherwise) definitely associated with the chromium ions in some, as yet unknown, manner. Further, detailed study of the saturation values at 0.47 μm for a number of Cr concentrations has been made and is plotted in figure 1. Absorbtivity at 0.47 μm is plotted vs. mol% Cr for a number of crystals. The ordinate is in arbitrary units, normalized only for sample thickness. This shows that the absorption coefficient reaches a broad maximum value at about 0.09 mol%. Novotny and Spurny [5] report similar results. It is to be noted that the "standard" pink laser ruby (0.05 wt %

Cr_2O_3) lies well down the curve at 0.034 % Cr. while the "red" ruby that oscillates above 0.7 μm (on the N lines rather than the R lines) lies well out in the tail near 0.34%. This marked reduction in susceptibility to damage with increasing chromium might suggest Cr pairing as being involved. The N lines, of course, are from Cr pairs; various authors have studied pairs, including for example Powell [6] and Gill [7].

The work of Stickley [1] indicates certain differences in detail between discoloration produced by laser pumping light and by ionizing radiation (i.e. x-rays). His work indicates that the longest wavelength band in pumped laser rods is near 0.4 μm and has a definite long wavelength tail extending out to at least 0.7 μm. He offers evidence that "his" bands are in fact the same bands produced in "pure" sapphire by ionizing radiation as described by Levy [8].

We have initiated experiments to produce and study these pumped (i.e. ultra-violet light produced) effects. Samples included "in house" crystals, and crystals from two different commercial sources, both being reputed to be particularly susceptible to pump discoloration. These were mounted in an uncooled ruby laser head, with no UV filter provided. The "head" was flashed at 2 minute intervals and samples measured for discoloration. To date, after some 300 flashes only slight coloration has been observed, but this is insufficient to be clearly outside the limit of experimental detectibility. Future work along these lines should be done, perhaps with cooling, with a stronger source, or perhaps with a strong CW mercury arc.

Electron paramagnetic resonance measurements have been made on a number of these samples. As indicated, special attention was given to a search for trace impurities of paramagnetic ions or other paramagnetic defects in general (i.e. color centers). Changes in the normal Cr^{3+} spectra were searched for with the intentions of correlation with the observed optical data. A very special effort was directed at finding the EPR band studied by Hoskins and Soffer [2] and by Mason and Thorp [3].

Included initially was a "pure" "in house" sapphire that showed a clear Cr^{3+} EPR spectra and no change on x-ray irradiation. A vapor phase grown sapphire, grown by another group at NBS, gave no Cr^{3+} EPR signal, attesting to its unusual purity in this respect. A number of rubies yielded the normal Cr^{3+} EPR spectra and no change after x-ray coloring.

Subsequent to the above, the Hoskins and Soffer line [2,3], which they attribute to Cr^{4+}, has been observed in this laboratory. Two laser quality samples of 0.05 and 0.01 wt % Cr_2O_3 were obtained from the Naval Research Laboratory (NRL). These had been colored by 10^6 R/ cm^2 sec. of ^{60}Co irradiation and carefully protected from all light except dim incandescent bulbs.

The prior difficulty in observing this line is not completely understood. It is possible that it is very easily bleached optically, and hence is not caused by the same mechanism responsible for the optical color. They are related of course since they have been shown to be generated both chemically (2), and by irradiation. The difficulty is believed, very definitely, to be related to lack of proper sample preparation in the earlier experiments. It is found necessary to operate at low temperature, 4.2K.

Figure 2 is the EPR line obtained on a 0.005 wt % sample grown here and irradiated by 2.6 x 10^8 (R/cm^2 sec.) of ^{60}Co. The magnetic field increases to the right, the "zero" signal level is indicated, and the position of the zero crossing (indicated) is chosen as the center of this unsymmetrical line. Nearby structure as well as the asymmetry indicate a line of some complexity. The center field of 0.176 Tesla and the frequency of 9.4671 GHz indicate a g_{eff} of 1.92, assuming a $\Delta m = 2$ transition. The power level into the cavity was 355 μ watts.

Figure 3 is that of the 0.05 wt % NRL sample showing the "line" at two power levels. The solid curve was taken at 355 μ watts, the dashed curve at 2.51 μ watts. Thus the extreme sensitivity of the sidebands of this line to power level is well illustrated. To study completely this line and its side bands, it is evident that the power levels required cover an extremely broad range. The lower end of this range can only be observed by an excellent superheterodyne detector such as is available in this laboratory.

The apparent lack of the appropriate structure would seem to rule out the existence of the normal hyperfine structure anticipated for Cr^{4+}, thus we currently find the identification with Cr^{4+} to be unsatisfactory. On the other hand the geometry of the cavity, viz. the $B_{dc}//B_{rf}//$ c-axis together with the rhombohedral field of the corundum lattice, would make the identification of the line with a $\Delta m = 2$ transition extremely likely. Finally, on cooling from 4.2K down to 1.7K the signal strength is reduced by a factor consistent with an activation energy of about 7 cm^{-1}. Thus we envision a spin 1 model in which

the ground state is spin 0 lying perhaps 7 cm^{-1} below the ± 1 states. The latter can be observed as a $\Delta m = 2$ transition under proper conditions. Of course, this is the model expected for Cr^{4+} but we currently rule this out for other reasons.

We have also given 2.6×10^8 R/cm^2 of ^{60}Co irradiation to several other samples of "in house" crystals, and as before, protected them from strong light. A "pure" sapphire crystal was found to contain Cr^{3+}, a trace of iron, and a weak $\Delta m = 2$ line, although the sample geometry was probably unfavorable in this case.

Also during this period both optical and EPR measurements were made on certain specially prepared samples of Nd glass to test these methods as means of detecting Pt inclusions. However, both the optical and EPR bands are too broad to permit reasonable sensitivity, and these methods do not seem very promising.

Future Plans

Experiments planned for the immediate future, some in fact under way, are outlined in the following list:

1. Work is to commence immediately on YAG. The obvious importance of rare earth doped YAG, together with the report of discoloration/degradation of YAG during laser operation, would seem to make such work significant. Damage will be produced by both optical pumping and ionizing radiation. Optical studies and EPR measurements will be made in order to get some understanding of the nature of this trouble. Greater emphasis will be placed on the infra-red than has been done in ruby. YAG (pure, Nd doped, and possibly double doped with Nd and Cr) will be included. Some appropriate material is in hand and more is expected shortly.

2. The EPR facilities to be employed are expected to include K - band capabilities soon. One bridge and a low temperature cavity set-up is nearly in operation. A K - band optical/EPR cavity has been designed that, hopefully, will soon be constructed. The use of optical/EPR cavities allows optical bleaching or excitation in the cavity. A true double resonance experiment has obvious application in the study of the ^2E excited state in ruby and it may prove useful in YAG. Lastly, double resonance of the excited state may be a means for meaningful EPR study of laser glass. It is possible that the excited state EPR bands may be narrow as contrasted with the broad ground state lines usually encountered. Successful work on

these latter problems will probably depend upon improvement in direct optical resolution, which is currently being planned, and upon use of K-band frequencies; the higher magnetic field will increase the optical splitting and also help in this respect.

3. Some work will continue on ruby, with special emphasis on the correlation between optical and EPR spectra, now that the $\Delta m = 2$ line seems to be readily available. The hydrogen bleaching of the orange coloration in Mg-doped ruby is most puzzling, and could well be explored further, such as by additional multiple doping experiments. The possibility of the easy optical bleaching of the $\Delta m = 2$ EPR line has not been examined as yet and will be shortly.

4. One interesting optical/EPR correlation experiment suggests itself, and will be attempted soon. The pronounced maximum in coloration with Cr concentration (fig. 1) could be correlated with the $\Delta m = 2$ line. These samples are still available and can readily be prepared for EPR work. In addition, the possibility of Cr pairing being involved can be explored by examining the EPR pair spectra discussed by Gill [7]. He found these lines at concentrations as low as 0.03 mol% and the signal increased quadratically with concentration.

5. Further efforts at coloration of various ruby samples with pumping light must be made and will involve a 1 KW mercury arc.

6. Two other experiments are contemplated. One involves a search for the expected 7 cm^{-1} band in the ground state of Cr^{4+} in colored ruby and the attendant Zeeman splitting of that low lying excited state. This must be done in the far infra-red. If it is done, it will be done at NRL and positive results would be most interesting. This work would follow similar work on other ions as reported by Joyce and Richards [9].

The second experiment will be a precision magnetic susceptibility measurement of the paramagnetic spins in ruby. This work would be done by G. A. Candela in this laboratory, using existing equipment [10]. The sensitivity available is believed to be more than adequate for precision measurements of the paramagnetic spin concentrations involved. The identification of any particular ion, which is absolutely essential for this method to be of any interest, would be done as follows. The susceptibility measurements are made on the sample while mounted in a special low temperature microwave cavity. Any ion, for example Cr^{3+}, that can be "saturated" at resonance, will

have its spin "removed" from the overall susceptibility. The net loss in susceptibility can then be used to calculate the Cr^{3+} concentration.

References

[1] C. M. Stickley, H. Miller, E. E. Hoell, C. C. Gallagher and R. A. Bradbury, J. Appl. Phys. 40, 1792 (1969).

[2] R. H. Hoskins and B. H. Soffer, Phys. Rev. 133, A490 (1964).

[3] D. R. Mason and J. S. Thorp, Proc. Phys. Soc. (G.B.) 87, 49 (1966).

[4] D. M. Dodd, D. L. Wood, and R. L. Barns, J. Appl. Phys. 35, 1183 (1964).

[5] J. Novotny and Zd. Spurny, Czechoslovak Jour. of Phys. 16B, 119 (1966).

[6] Richard C. Powell, B. DiBartolo, B. Birang, and C. S. Naiman, Phys. Rev. 155, 296 (1967).

[7] J. C. Gill, Proc. Phys. Soc. (G.B.) 79, (Pt. 1), 58 (1962).

[8] Paul W. Levy, Phys. Rev. 123, 1226 (1961).

[9] R. R. Joyce and P. L. Richards, Phys. Rev. 179, 375 (1969).

[10] G. A. Candela and R. E. Mundy, Rev. Sci. Instr. 36, 338 (1965).

USCOMM—NBS—DC

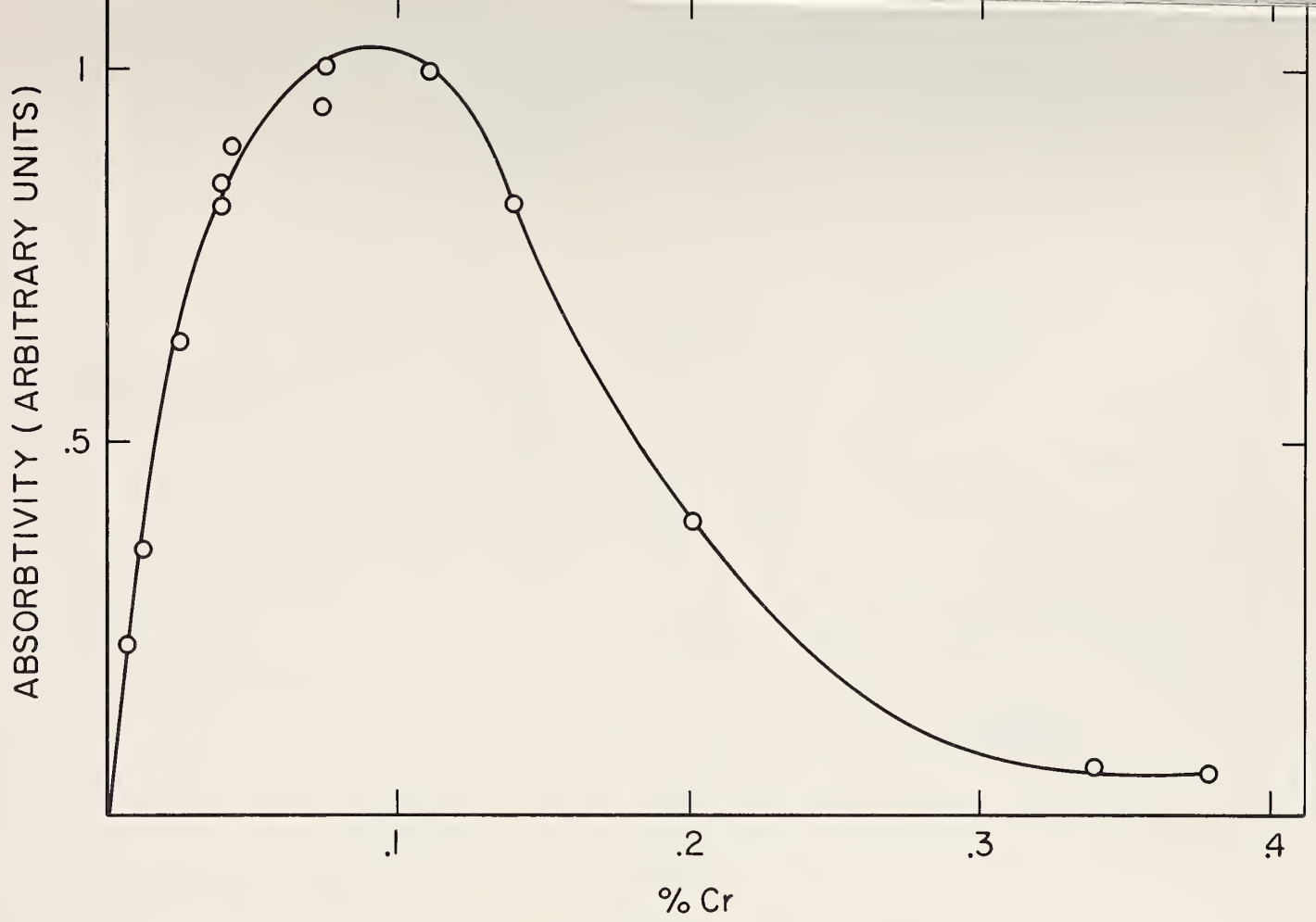

Figure 1. Added coloration at 0.47 μm (E ⊥ C) plotted vs. mol % Cr for ruby crystals irradiated to saturation with X-rays. The ordinate is in arbitrary units normalized for sample thickness.

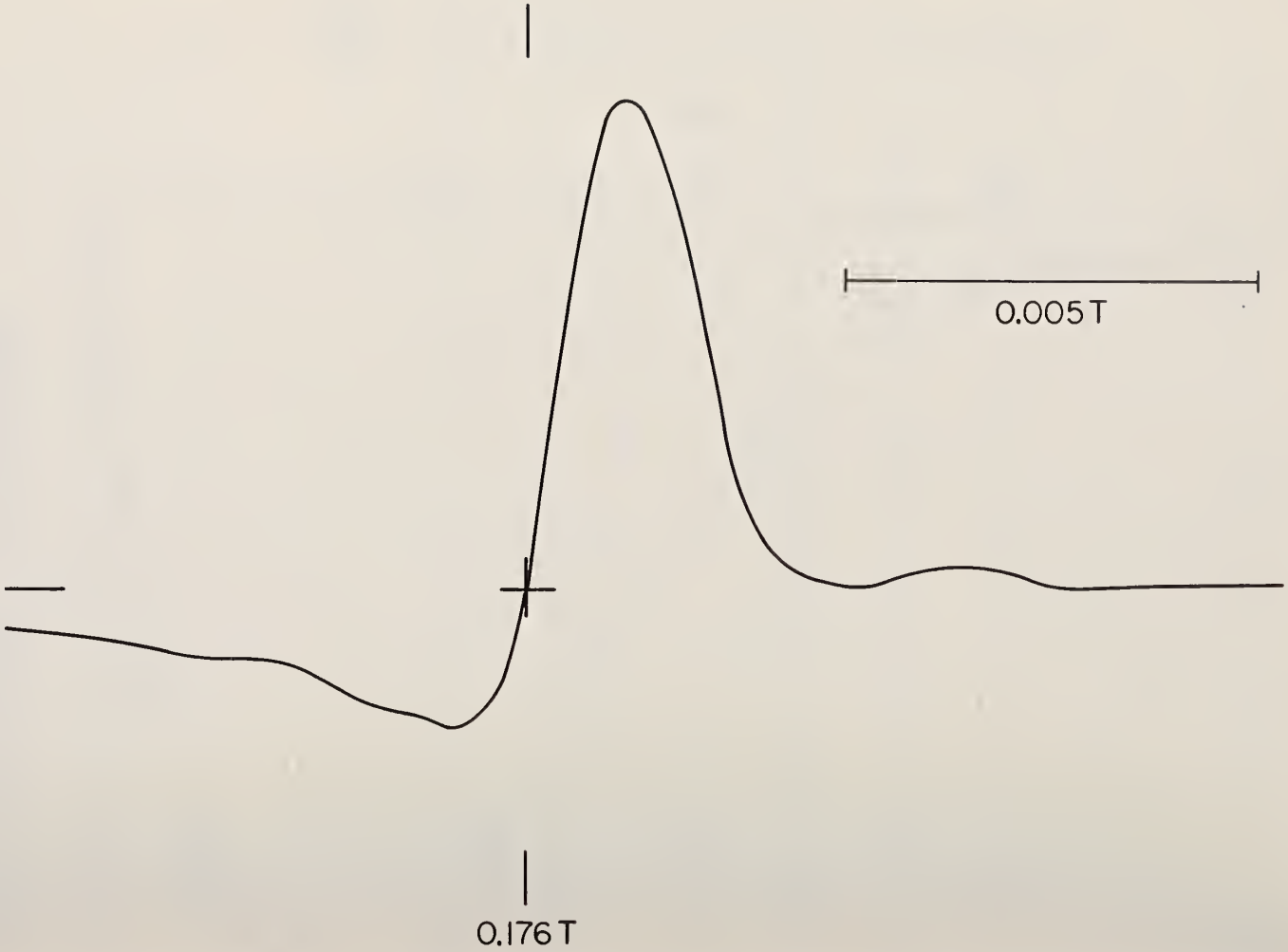

Figure 2. The $\Delta m = 2$ EPR line produced by ^{60}Co irradiation on a 0.005 wt % ruby sample. $g_{eff} = 1.92$. The applied magnetic field increases to the right.

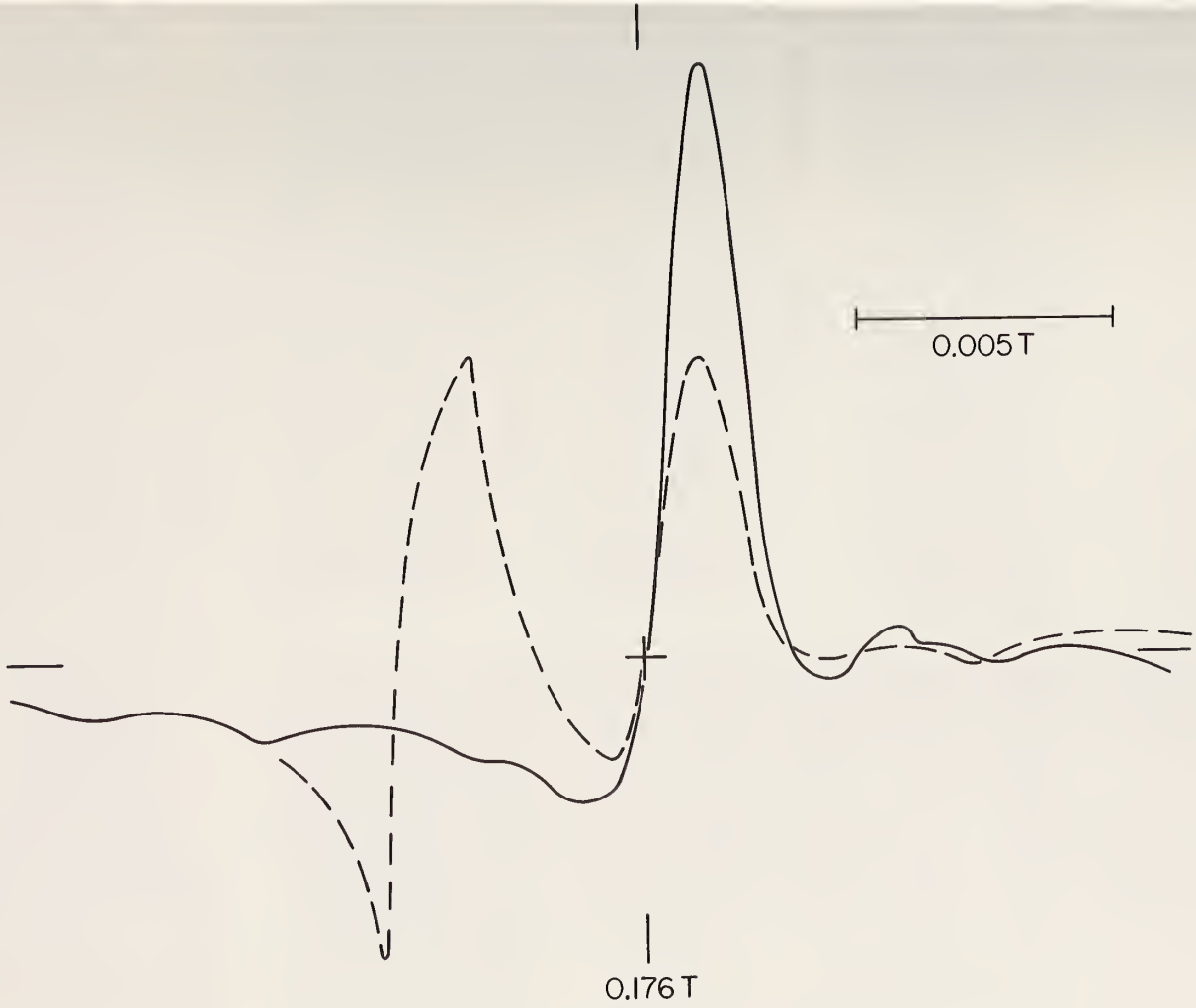

Figure 3. The $\Delta m = 2$ EPR line from a ^{60}Co irradiated 0.05 wt % ruby taken at 355 μ watts (solid curve) and 2.51 μ watts (dashed curve). The applied magnetic field increases to the right.

NBS TECHNICAL PUBLICATIONS

PERIODICALS

JOURNAL OF RESEARCH reports National Bureau of Standards research and development in physics, mathematics, chemistry, and engineering. Comprehensive scientific papers give complete details of the work, including laboratory data, experimental procedures, and theoretical and mathematical analyses. Illustrated with photographs, drawings, and charts.

Published in three sections, available separately:

• Physics and Chemistry

Papers of interest primarily to scientists working in these fields. This section covers a broad range of physical and chemical research, with major emphasis on standards of physical measurement, fundamental constants, and properties of matter. Issued six times a year. Annual subscription: Domestic, $9.50; foreign, $11.75*.

• Mathematical Sciences

Studies and compilations designed mainly for the mathematician and theoretical physicist. Topics in mathematical statistics, theory of experiment design, numerical analysis, theoretical physics and chemistry, logical design and programming of computers and computer systems. Short numerical tables. Issued quarterly. Annual subscription: Domestic, $5.00; foreign, $6.25*.

• Engineering and Instrumentation

Reporting results of interest chiefly to the engineer and the applied scientist. This section includes many of the new developments in instrumentation resulting from the Bureau's work in physical measurement, data processing, and development of test methods. It will also cover some of the work in acoustics, applied mechanics, building research, and cryogenic engineering. Issued quarterly. Annual subscription: Domestic, $5.00; foreign, $6.25*.

TECHNICAL NEWS BULLETIN

The best single source of information concerning the Bureau's research, developmental, cooperative and publication activities, this monthly publication is designed for the industry-oriented individual whose daily work involves intimate contact with science and technology—*for engineers, chemists, physicists, research managers, product-development managers, and company executives.* Annual subscription: Domestic, $3.00; foreign, $4.00*.

* Difference in price is due to extra cost of foreign mailing.

NONPERIODICALS

Applied Mathematics Series. Mathematical tables, manuals, and studies.

Building Science Series. Research results, test methods, and performance criteria of building materials, components, systems, and structures.

Handbooks. Recommended codes of engineering and industrial practice (including safety codes) developed in cooperation with interested industries, professional organizations, and regulatory bodies.

Special Publications. Proceedings of NBS conferences, bibliographies, annual reports, wall charts, pamphlets, etc.

Monographs. Major contributions to the technical literature on various subjects related to the Bureau's scientific and technical activities.

National Standard Reference Data Series. NSRDS provides quantitive data on the physical and chemical properties of materials, compiled from the world's literature and critically evaluated.

Product Standards. Provide requirements for sizes, types, quality and methods for testing various industrial products. These standards are developed cooperatively with interested Government and industry groups and provide the basis for common understanding of product characteristics for both buyers and sellers. Their use is voluntary.

Technical Notes. This series consists of communications and reports (covering both other agency and NBS-sponsored work) of limited or transitory interest.

Federal Information Processing Standards Publications. This series is the official publication within the Federal Government for information on standards adopted and promulgated under the Public Law 89–306, and Bureau of the Budget Circular A–86 entitled, Standardization of Data Elements and Codes in Data Systems.

CLEARINGHOUSE

The Clearinghouse for Federal Scientific and Technical Information, operated by NBS, supplies unclassified information related to Government-generated science and technology in defense, space, atomic energy, and other national programs. For further information on Clearinghouse services, write:

Clearinghouse
U.S. Department of Commerce
Springfield, Virginia 22151

Order NBS publications from:

Superintendent of Documents
Government Printing Office
Washington, D.C. 20402

U.S. DEPARTMENT OF COMMERCE
WASHINGTON, D.C. 20230

OFFICIAL BUSINESS

POSTAGE AND FEES PAID
U.S. DEPARTMENT OF COMMERCE